Assessment of Potential Impact of Electromagnetic Fields from Undersea Cable on Migratory Fish Behavior

Period Covering: January 2014 - June 2016

Final Technical Report, September 2016

DOE Award Number: DE-EE0006382

ACKNOWLEDGMENTS

The following organizations, under contract to the Electric Power Research Institute (EPRI), prepared this report:

Principal Investigators
R. Kavet, Electric Power Research Institute, Environment Sector
M.T. Wyman, University of California, Davis, Department of Fish, Wildlife, & Conservation Biology
A. P. Klimley, University of California, Davis, Department of Fish, Wildlife, & Conservation Biology

Project Manager
X. Vergara, Electric Power Research Institute, Environment Sector

This report describes research sponsored by The Department of Energy and the Bureau of Ocean Energy Management under award number: DE-EE0006382.

EXECUTIVE SUMMARY

The US Department of Energy and US Department of the Interior, Bureau of Ocean Energy Management commissioned this study to address the limited scientific data on the impacts of high voltage direct current cables on aquatic biota, in particular migratory species within the San Francisco Bay. The study was conducted in several stages as described in three separate technical manuscripts which capture the methods, findings and recommendations. A summary of each manuscript is provided herein.

Objectives and Results

Empirical evidence exists that marine animals perceive and orient to local distortions in the earth's main geomagnetic field magnetic field. The electromagnetic fields generated by the cables that carry electricity from hydrokinetic energy sources to shore-based power stations may produce similar local distortions in the earth's main field. Concern exists that animals that migrate along the continental shelves might orient to the EMF from the cables, and move either inshore or offshore away from their normal path. The Trans Bay Cable (TBC) is a ±200-kilovolt (kV), 400 MW 85-km long High Voltage Direct Current (DC) buried transmission line linking Pittsburg, CA with San Francisco, CA (SF) through the San Francisco Bay. The study addresses the following specific questions based on measurements and projections of the EMF produced by an existing marine cable, the Trans Bay Cable, in San Francisco Bay.

- Does the presence of EMF from an operating power cable alter the behavior and path of bony fishes and sharks along a migratory corridor?
- Does the EMF from an operating power cable guide migratory movements or pose an obstacle to movement?

To meet the main study objectives several activities needed to be carried out: 1) modeling of the magnetic fields produced by the Trans Bay Cable, 2) assessing the migratory impacts on Chinook salmon smolts (*Oncorhynchus tshawytscha)* and green sturgeon (*Acipenser medirostris*)

as a result of local magnetic field distortions produced by bridge structures and 3) analyzing behavioral responses by migratory Chinook salmon and green sturgeon to a high-voltage power cable.

Modeling Magnetic Fields from a DC Power Cable Buried Beneath San Francisco Bay Based on Empirical Measurements

In July and August 2014, magnetic field measurements were made using two submerged Geometrics magnetometers towed behind a survey vessel in four locations in the San Francisco estuary along profiles crossing the cable path. We applied basic formulas to describe magnetic field from a DC cable summed vectorially with the background geomagnetic field (in the absence of other sources that would perturb the ambient field) to derive characteristics of the cable not immediately or otherwise observable. The magnetic field profiles of 76 survey lines were regressed against the measured fields, representing eight days of measurement. Many profiles were dominated by field distortions caused by bridge structures or other submerged objects, and the cable contribution to the field was not detectable (the the San Francisco-Oakland Bay Bridge did not yield usable data). The modeled field anomalies due to the cable, defined as the difference between the maximum and minimum field along the survey line at the cable crossing, was virtually identical to the measured values. The modeling yielded a pooled cable depth below the bay floor of 1.27 m (±0.14 std error), and estimated the angle to the horizontal of the imaginary line connecting the cross-sectional center of the cable's two conductors (0.1143 m apart) as 81.1°±8.1° (std dev) for Richmond-San Rafael Bridge, 118.5°±9.1° (std dev) for San Pablo Bay, and 184.6° ±70.7° (std dev) for the Benicia-Martinez Bridge. For the eight days, the mean of the daily average currents derived from the regressions was 823 ±208 A (std dev), as compared to 722 ±95 A (std dev) provided by Trans Bay Cable. The regressions based on fundamental principles (Biot Savart law) and the vectorial summation of cable and geomagnetic fields provide estimates of cable characteristics consistent with plausible expectations.

Chinook salmon and green sturgeon migrate through San Francisco Estuary despite large distortions in the local magnetic field produced by bridges

Based on a detailed gradiometer survey, we found that the distortions in the earth's main field produced by bridges across the estuary were much greater than those from the Trans Bay Cable. The former anomalies exceeded the latter by an order of magnitude or more. A total of 1025

smolts with ultrasonic beacons placed on them from 2007-2011 were detected passing under the Benicia Bridge and entering San Francisco Bay. Significant numbers of tagged Chinook salmon smolts migrated past bridges, which produced strong magnetic anomalies, to the Golden Gate Bridge, where they were recorded by dual arrays of acoustic tag-detecting monitors moored in lines across the mouth of the bay. In addition, a total of 74 inbound migration trips and 150 outbound migration trips by adult green sturgeon were monitored from 2007 to 2014. Adult green sturgeon successfully swam upstream and downstream through the estuary on the way to and from their spawning grounds. Hence, the large anomalies produced by the bridges that run perpendicular to these migration routes do not appear to present a strong barrier to the natural seasonal movement patterns of salmonid smolts and adult green sturgeon.

Behavioral responses by migratory Chinook salmon and green sturgeon to a high-voltage power cable

We have studied the effect of the Trans Bay Cable (TBC), an 85-km long high voltage direct current transmission line leading from Pittsburg, CA to San Francisco, CA, on fishes migrating through the San Francisco Estuary. These included late-fall run Chinook salmon smolts (*Oncorhynchus tshawytscha*) that migrate downstream through the San Francisco Estuary to the Pacific Ocean and adult green sturgeon (Acipenser medirostris), which migrate upstream from the ocean through the estuary to their spawning habitat in the upper Sacramento River and return to the ocean after spawning occurs. Detections from 763 late-fall Chinook salmon smolts were available from 2007 through 2011. After the cable was activated, there was an average increase of approximately 20% in both the proportion of Chinook smolts that crossed the cable location and the proportion of smolts detected at Bay Bridge south of their normal migration route. When comparing all years of data during cable inactivity (2007-2009) versus activity (2011), cable activation was associated with an average decrease of 11.1 % in the proportion of Chinook smolts that were able to successfully exit San Francisco Bay. Cable activity did not predict an increase in the probability of crossing the cable location or in successfully exiting the system, but it did predict an increase in the probability that LFC smolts would be misdirected to Bay Bridge. Cable activity was also not significantly related to transit time in any of the three reaches of this system. Furthermore, relationships between cable activity and transit rate in late-fall run Chinook were not robust. Lastly, after the cable was activated, distance to cable remained the

only significant factor predicting the first detection location of Chinook smolts at an array. Our results indicate Chinook salmon smolts may be attracted to the cable after activation (more cable location crossings, more detections at Bay Bridge, high importance of distance to cable in predicting fish location), but are not impeded from successfully migrating through the San Francisco Bay (similar proportions of successful exits, faster transit rates). In outbound migrating adult green sturgeon, cable activation was associated with a 14.9 % increase in the proportions of migrations that crossed the cable location, a 2.3 % increase in the proportion of migrations that involved detections at Bay Bridge, and a 4.0 % decrease in the proportion of successful migrations (i.e., detections at Golden Gate). Transit times of outbound migrations from Carquinez to Golden Gate were not affected by crossing the cable location but were trending towards being longer if the fish was detected at Bay Bridge and were significantly longer after cable activation versus before activation. For inbound migrating adult green sturgeon, periods of cable activity were associated with a 6.5 % decrease in the proportion of migrations that involved detections at Bay Bridge and a 1.5 % increase in the proportion of successful inbound migrations (i.e., detections at Carquinez). Cable activity had opposite effects on outbound and inbound green sturgeon migrations: outbound migrations had significantly longer transit times while inbound migrations had significantly shorter migration times. However, the proportion of green sturgeon that successfully migrated through the San Francisco Bay was not strongly impacted after cable activation for either migration type.

Summary

Based on the work carried out in this study, we provide the following conclusions:

1. The mean values of twist angle, Θ, cable depth, a, and load current, I, derived from the regressions appear to bear a consistency with what one could expect from direct observation of these parameters. Calculations of magnetic fields for assessment of marine life can be performed; however, local anomalies in the fields resulting from submerged structures require validation of such calculations through collection of ambient DC magnetic field data.

2. The large anomalies produced by the bridges that run perpendicular to these migration routes do not appear to present a strong barrier to the natural seasonal movement patterns of salmonid smolts and adult green sturgeon.

3. Chinook salmon smolts may be attracted to the activated cable based on analysis of cable crossing, mis-directions, and first presence at the array data, however, the cable activation does not appear to change the proportion of smolts that successfully migrate through the San Francisco Bay. Cable activation has different impacts on inbound and outbound migrating adult green sturgeon: travel time was increased for outbound migrations but decreased for inbound migrations. However, cable activation did not appear to impact the success of either migration type in this species.

CONTENTS

LIST OF FIGURES

LIST OF TABLES

2
MODELING MAGNETIC FIELDS FROM A DC POWER CABLE BURIED BENEATH SAN FRANCISCO BAY BASED ON EMPIRICAL MEASUREMENTS

Introduction

The Trans Bay Cable (TBC) is a ±200-kilovolt (kV) 85-km long High Voltage Direct Current (DC) submerged transmission line linking Pittsburg, CA with San Francisco, CA (SF) through the San Francisco Bay (Figure 2-1). The cable operates at a nominal power of 400 megawatts (MW); thus, the cable is rated to operate with an approximate nominal load current of 1,000 ampere (A). The current produces a DC magnetic field in the proximity of the cable; however, the cable is clad in a conductive sheath that shields the electric field the cable would otherwise produce (Figure 2-1, inset). With the expected rise of offshore electric power generation with associated transport of electricity through buried cables such as these, there is heightened interest in assessing how anthropogenic magnetic fields may impact the behaviors species with magnetosensitivity [1]. The TBC runs parallel or perpendicular (depending on the location) to the migratory route of various anadromous species that spend their most of their adult life in the ocean, but migrate upstream to spawn in rivers. Adult Chinook salmon *Oncorhynchus tshawytscha*, steelhead trout *Oncorhynchus mykiss* [2] and green sturgeon *Acipenser medirostris* [3, 4] migrate from the Pacific Ocean through the San Francisco Bay to their spawning destinations further upstream in the Sacramento-San Joaquin Watershed. After spawning, steelhead trout and green sturgeon transit back through the bay on their way to their feeding grounds in the ocean and along the coast. Juvenile Chinook salmon *Oncorhynchus tshawytscha* [5, 6] and steelhead trout [4, 7] also migrate from the upstream rivers to the ocean. Studies have indicated that species within the salmonid [8-11] and sturgeon families [12-14] may use the natural ambient magnetic (or electric) fields to guide their movements during migration or foraging behaviors. Under an award from the U.S. Department of Energy researchers at the Electric Power Research Institute in Palo Alto, CA and the University of California at Davis are

addressing whether the presence of the TBC affects migratory patterns of these anadromous species as they pass through the San Francisco Estuary (SFE). In the current context, the cable is serving as a surrogate for assessing potential magnetic field effects associated with marine hydrokinetic technologies.

Figure 2-1 The Trans Bay Cable route (thick blue line) from Pittsburg, CA (upper right) to San Francisco, CA (lower left) showing locations of magnetometer surveys (red lines):

(1) Benicia-Martinez Bridge (Ben), (2) San Pablo Bay (SP), (3) Richmond-San Rafael Bridge (RSR), and (4) San Francisco-Oakland Bay Bridge (BB). The migration route of anadromous fish runs between the Sacramento-San Joaquin Delta (upper right) and the mouth of the Pacific Ocean (lower left). The inset shows a cross-section of the cable with a total diameter of 11.43 cm (note it is clad in a metallic sheath, which shields electric fields).

In July and August 2014, an extensive series of magnetic field measurements were taken by a pair of submerged Geometrics magnetometers towed behind a survey vessel in four locations in the SF estuary along profiles that cross the cable's path (Figure 2-1). In this paper, we apply basic formulas that ideally describe the magnetic field from a DC cable summed vectorially with the background geomagnetic field (in the absence of other sources that would perturb the ambient field) to derive characteristics of the cable that are otherwise not immediately observable. A consistency of the measured with the derived profiles would provide assurance

that magnetic fields could be predicted for a specific set of cable conditions and configurations relevant to a previous date and location of interest with respect to fish migratory behavior.

Methods

Study Site and Data Collection

A series of underwater magnetic field measurements were made in July and August 2014 along pre-defined paths that transected the cable at four locations: San Francisco-Oakland Bay Bridge (BB), the Richmond-San Rafael Bridge (RSR) and the Benicia-Martinez Bridge (Ben), as well as in an area in San Pablo Bay (SP) in which a bridge is not present (Figure 2-1). Survey lines were designed to run parallel to pre-existing cross-channel arrays of fish detecting acoustic hydrophones deployed in the San Francisco Bay along the BB, RSR, and Ben bridges and in San Pablo Bay. Most of these survey lines crossed the cable perpendicularly, except where the cable's path curved within the surveyed site. These lines extended along the entire span of the bridges (as far towards the banks as possible) and at least 1 km outwards from the fish detection array in San Pablo Bay. Survey lines started as close to the bridge/array as possible on each side and were repeated every 100 m away from the bridge/array up to 1 km. Twenty to 24 survey lines were delineated at each location. These field surveys were conducted with the approval of the US Department of Energy under the National Environmental Policy Act.

To acquire magnetic field data, a G-882 Transverse Gradiometer (TVG) (Geometrics, Inc., San Jose, CA), consisting of a pair of cesium magnetometers (0.004 nT/√Hz RMS) separated by 1.5 m, two depth sensors, and an altimeter, was deployed into the water and towed behind the survey vessel. MagLog magnetic data acquisition software (Geometrics, Inc.) was used to design the survey line tracks, accurately navigate the boat, and integrate the data streams during field measurements. The sampling rate was set at 10 Hz and magnetic field measurements were geo-referenced using a Trimble GeoExplorer XT Global Positioning System (GPS) with Hurricane LI antenna (Trimble Navigation Limited, Sunnyvale, CA).Two types of tows were conducted on each survey line. 'Surface tows', with the TVG towed at a depth of 0.5 and 3 m, were conducted along the full length of each survey line. Additional 'deep tows' were conducted in areas where the TVG during surface tows were more than 10 m above the channel bottom.

After field surveys were completed, MagPick magnetometer data processing software (Geometrics, Inc., http://sourceforge.net/projects/magpick/) was used to post-process and map

the magnetic field data. Post-processing included 1) differentially correcting the GPS points to get submeter accuracy on survey positions, 2) correcting for tidal stage (based on tidal stage data downloaded from the nearest port station operated by the *National Oceanic and Atmospheric Administration, NOAA*), 3) correcting for fluctuations in the Earth's magnetic field (by subtracting daily measurements of the Earth's field made by the total-field magnetic field observatory at Jasper Ridge Biological Preserve from our field measures), and 4) removing HVDC offset between the two magnetometers on the TVG. After post-processing, the survey line profiles were used to map local magnetic field anomalies at each location for both the surface and the deep tows (Figure 2-2).

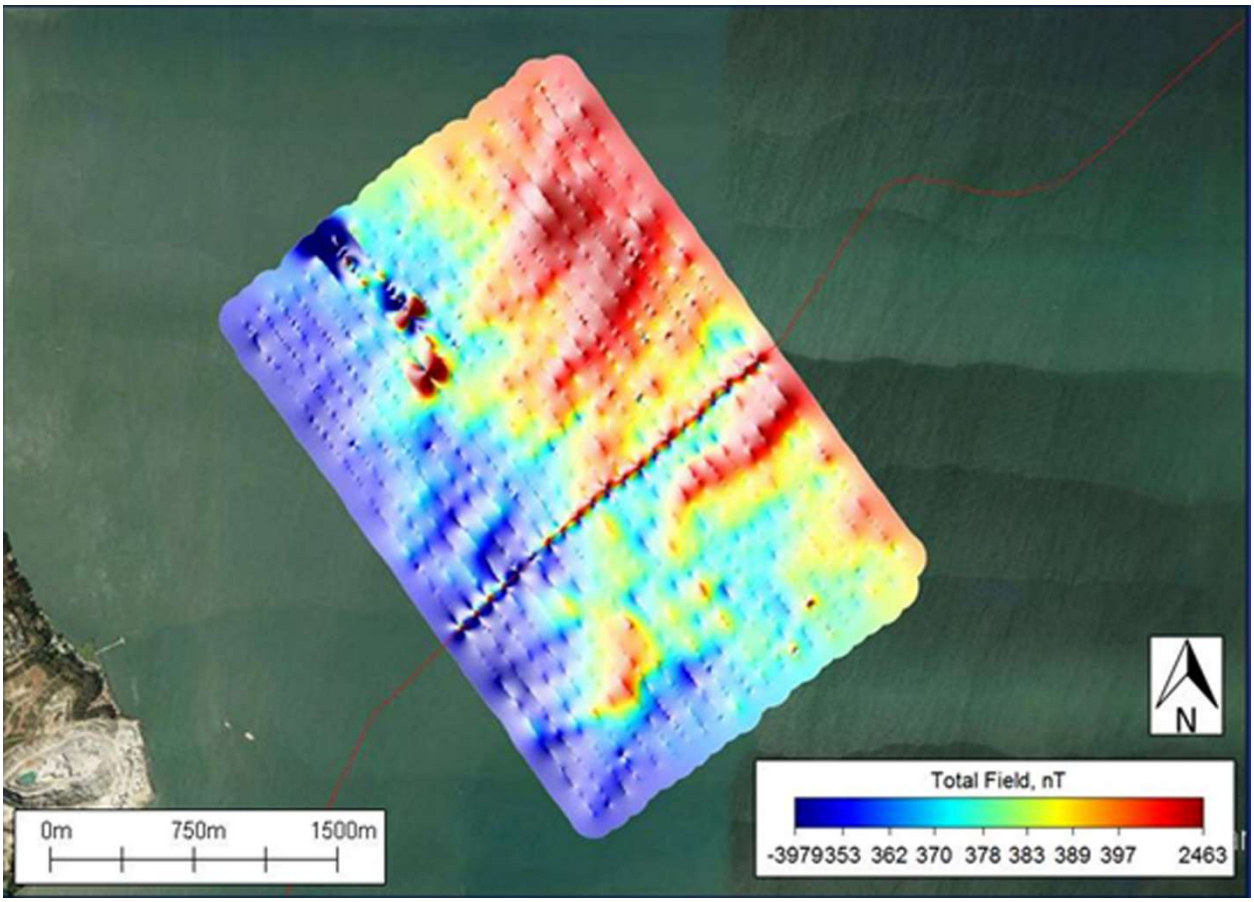

Figure 2-2 Local magnetic field map of San Pablo Bay generated by surface tow profiles.

The path of the cable, indicated by the line of small spikes in nT, can be seen running through the middle of the magnetic field map in a southwesterly direction.

Magnetic Field Calculation

The magnetic fields attributable to the load on the TBC can be calculated with the Biot-Savart law, and are broken down to vertical, east and north components, which sum as vectors with the geomagnetic field. In the SFE, the field has a total magnitude of about 48,800 nT, with a vertical component (i.e., perpendicular to the Earth's plane) of about 42,800 nT, pointing into the Earth (down); a component pointing east with a magnitude of about 5,600 nT; and a component pointing north with a magnitude of about 22,700 nT. The subscripts in the following notation indicate the magnetic field (*B*) source, *Geo* for the geomagnetic field, *Cable* for the TBC, with each followed by their directional component, *North*, *East* or *Vertical*. The magnitude of the geomagnetic field, also known as its *resultant*, $B_{GeoTotal}$, is calculated as,

$$B_{GeoTotal} = \sqrt{(B_{GeoNorth}^2 + B_{GeoEast}^2 + B_{GeoVertical}^2} \text{ nT} \quad (1)$$

The combined *Geo* and *Cable* magnetic field resultant, B_{Total}, is,

$$B_{Total} = \sqrt{(B_{CableNort}^2 + B_{GeoNorth}^2) + (B_{CableEast}^2 + B_{GeoEast}^2) + (B_{CableVertical}^2 + B_{GeoVertical}^2)} \text{ nT} \quad (2)$$

The *Net*, that is, the amount that the magnitude of the local field near the TBC deviates from the magnitude of the geomagnetic field is,

$$B_{Net} = B_{Total} - B_{GeoTotal} \text{ nT} \quad (3)$$

The parameters used to describe the magnetic field attributable to the TBC using the Biot-Savart law are listed in Table 2-1, with a description of parameters Θ and Φ shown in Figure 2-3.

Table 2-1 Parameters for computing field from DC cable

Parameter	Symbol	Units
Current	I	Amps (A)
Conductor separation	s	meters (m)
Height of magnetometer above bottom	ALT	m
Buried depth of cable	a	m
Lateral distance of magnetometer along the survey line from vertical projection of cable	x	m
Cable twist (Figure 2-4)	Θ	radians (degrees)
Profile angle relative to East-West (Figure 2-4)	Φ	radians (degrees)
North component of earth field	$B_{GeoNorth}$	nT
East component of earth field	$B_{GeoEast}$	nT
Vertical component of earth field	$B_{GeoVertical}$	nT

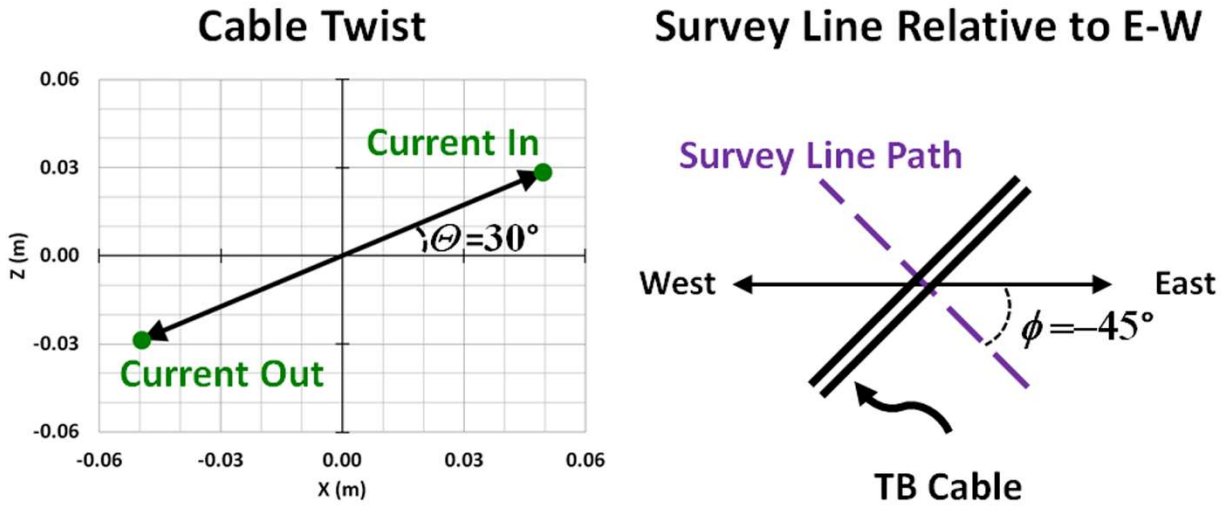

Figure 2-3 Definition of the angle of cable twist (Θ), and the angle of the lateral survey line relative to geographic East-West (Φ).

The centers of the two cross-sections of the conductors that comprise the cable are 0.1143 meters (m) apart (4.5 inches) (s in Table 2-1). Two examples of the dependence of the field profile on Θ and Φ are illustrated in Figure 2-4; the examples assume the following values (and assumes the survey line's path is exactly perpendicular to the cable):

I = 1,000 A

s = 0.1143 m

ALT+a = 5 m (that is, the total vertical height to the measurement point from the cable)

$B_{GeoTotal}$ = 48,677 nT (horizontal broken line)

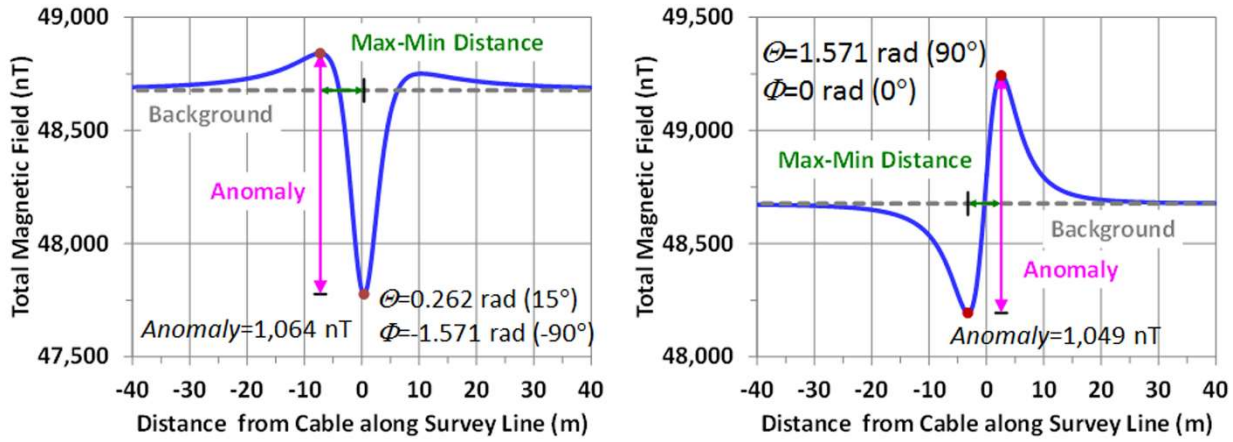

Figure 2-4 The total magnetic field for two sample profiles (5 m above the cable, loaded to 1,000 A).

The graphs indicate the magnitude of the anomaly and the distance between field minima and maxima. The anomaly's magnitude is measured as the difference between the maxima and minima of the total magnetic field values. The examples illustrate the variability of the profiles with different values of Θ and Φ.

The cable '*Anomaly*' is the perturbation in the ambient magnetic field produced by the cable. Its magnitude is the difference between the maximum and the minimum net magnetic field along the survey line at the cable crossing. Note that for these examples, meant to represent nominal load conditions, the field decays to background by ~±40 m lateral distance from the vertical projection of the center of the cable.

Results

The Sample

The results presented below include measurements taken at three locations on eight separate days in 2014 from July 10 to August 7. Two sets of measurements were taken at each location, one closer to the surface (S), and another at a greater depth (D); thus, for example, the deep measurements at San Pablo Bay would be identified by SP-D. The breakdown of survey line profiles by location and date is shown in Table 2-2, indicating the number of profiles measured and the number with sufficient structure at the anomaly to be regressed. Anomalies unrelated to the DC cable could be up to roughly 100 times greater than the anomaly associated with the cable. Only two of the 40 profiles at BB were regressed, and the BB profiles were not considered further in the results. For the other three locations, 76 out of a total of 130 measured profiles were fitted (58.5%).

Table 2-2 Survey Line Profiles: Dates Measured and Number Regressed

Group	Date	Number of Profiles Measured	Number of Profiles Regressed	Percent
BB-D	8/6	2	0	0.0%
BB-D	8/8	16	2	12.5%
BB-D	8/9	2	0	0.0%
BB-S	7/16	9	0	0.0%
BB-S	7/17	9	0	0.0%
BB-S	7/25	2	0	0.0%
Ben-D	8/7	24	7	29.2%
Ben-S	8/7	24	9	37.5%
RSR-D	8/1	11	7	63.6%
RSR-D	8/4	9	7	77.8%
RSR-S	7/10	10	4	40.0%
RSR-S	7/15	10	7	70.0%
SP-D	7/29	2	2	100.0%
SP-D	7/31	19	18	94.7%
SP-S	7/28	13	10	76.9%
SP-S	7/29	8	5	62.5%
	All	170	78	45.9%
	w/o BB	130	76	58.5%

BB, San Francisco-Oakland Bay Bridge; Ben, Benicia-Martinez Bridge; RSR, Richmond-San Rafael Bridge; SP, San Pablo Bay. Suffixes represent measurement depth: D, Deep; S, Surface.

With the exception of Ben-S, whose profiles analyzed included between 401 and 601 data points across an average distance of 144 m, the other sites had profiles consisting of between roughly 800 and 2,500 data points across distances of 166 m to 300 m (Table 2-3). The average distance between measurement points for each group (organized by location and tow depth) ranged between 0.15 m/measurement to 0.26 m/measurement with the minima and maxima shown in Table 2-3. The average height of the magnetometers above the bottom of the water, ALTavg (m), remained at a stable value across all three locations (Table 2-4). Two examples of the curve-fitting results for profiles displaying a discernible anomaly are shown in Figure 2-5. In general all of the fits were similar in nature to those shown in the max-min region of the curves, but several fits diverged at the right and/or left tail (probably attributable to unrelated, but unidentifiable sources).

Table 2-3 Summary Characteristics of Survey Line Profiles Regressed

Group	N Profiles	N Meas.	Profile Distance (m)	Dist/Meas (m)
Ben-D	7	1492 (1393-1601)*	217 (166-250)	0.15 (0.10-0.17)
Ben-S	9	423 (401-601)	144 (128-202)	0.34 (0.32-0.38)
RSR-D	14	1368 (1256-1489)	228 (199-300)	0.17 (0.13-0.20)
RSR-S	11	1026 (790-1263)	258 (200-300)	0.26 (0.19-0.38)
SP-D	20	1611 (887-2474	260 (200-300)	0.17 (0.08-0.23)
SP-S	15	1215 (962-1474)	271 (200-300)	0.23 (0.15-0.31)
All	76	1252 (401-2474)	238 (128-300)	0.21 (0.08-0.38)

* Mean (Min-Max Range)

Table 2-4 Modeled Mean Twist Angle, Θ (deg), by Location and Depth of Measurement

	Deep (1)		Surface (0)		Pooled	
Location	N	Mean ±sd	N	Mean ±sd	N	Mean ±sd
Ben	7	164.2±74.6	9	200.6±67.5	16	184.6±70.7
RSR	14	81.9±6.2	11	80.1±10.2	25	81.1±8.1
SP	20	117.4±9.7	15	120.0±8.5	35	118.5±9.1

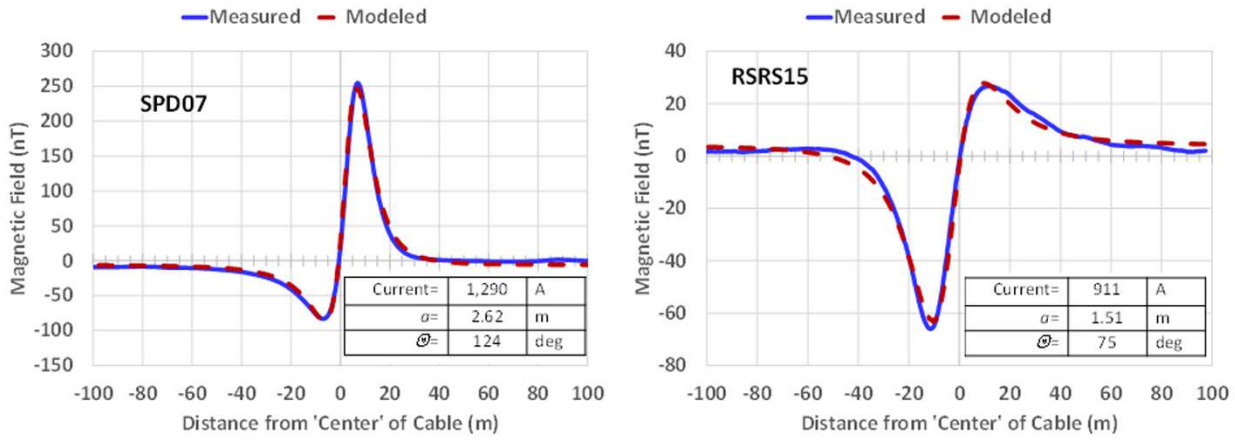

Figure 2-5 Two examples of the measured and modeled net magnetic field (B_{net}).

The derived values of current (I), cable depth (a), and twist angle (Θ) are shown in the insets. (SPD07, San Pablo Bay Deep, Profile #7;RSRS15, Richmond San Rafael bridge Surface, Profile #15).

Anomaly

A primary result of the exercise is that the measured and modeled values of the anomalies were virtually identical, with a pooled slope of unity (Pearson correlation, r=0.999) when plotted against each other and a pooled intercept consistent with the origin (Figure 2-6). Ben-S was censored for comparing the modeled values of max-min distance (Figure 2-7) to the measured values because their profiles were notably shorter than those from the other groups (Table 2-3), and the observed anomalies did not appear to have well defined minima (dealt with further in Discussion). For the other five groups the modeled absolute max-min distances were highly correlated to the observed absolute values (r=0.97), but the modeled values were on the average 6.3% lower than those measured (t-test, comparing slope to 1.0; p<0.05, df=65), although the intercept of the linear regression is consistent with the origin.

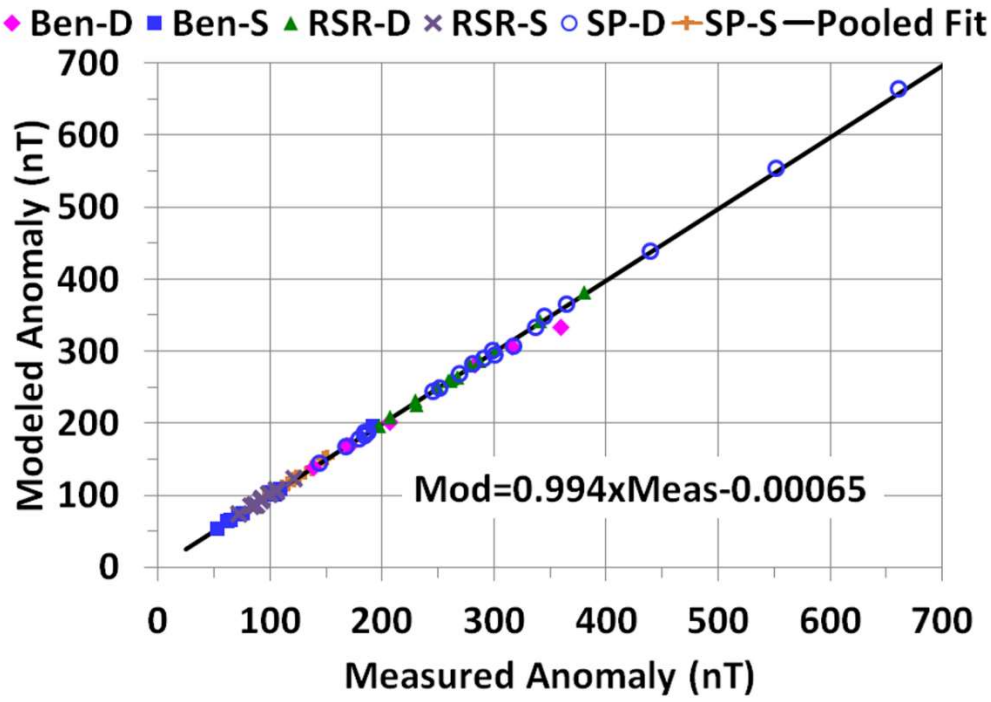

Figure 2-6 Modeled versus measured anomaly by data set group.

The regression line represents all points pooled.

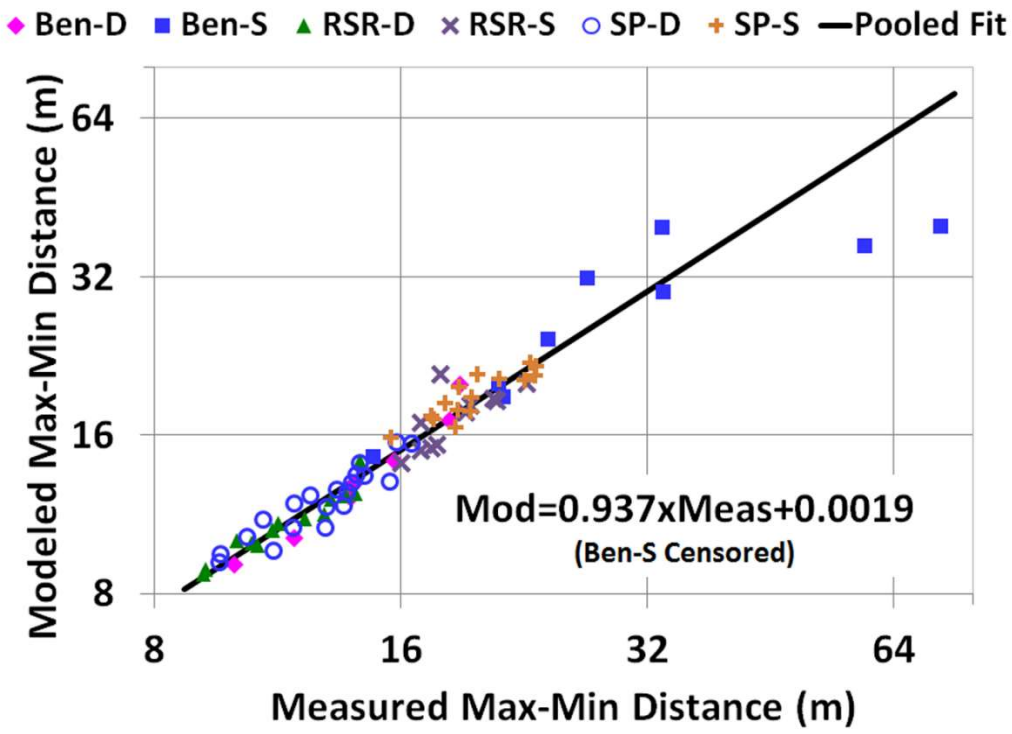

Figure 2-7 Modeled versus measured min-max distance by data set group.

The regression line represents all points pooled with the exception of Ben-S (see Discussion).

Twist Angle, Θ, and Cable Depth, *a*

Besides the separation of the cable's two conductors (0.1143 m for its entire route), the other two physical descriptors of the cable that are relevant to the magnetic field, but are not observable in any practical way, are its twist angle, Θ (deg) and buried depth, *a* (m) (see Tables 2-4 and 2-5 for descriptive statistics summarizing the regression results).

Table 2-5 Modeled Mean Cable Depth, *a* (m), by Location and Measurement Depth

	Deep (1)		Surface (0)		Pooled	
Location	N	Mean ±sd	N	Mean ±sd	N	Mean ±sd
Ben	7	0.45±0.95	9	1.29±2.07	16	0.92±1.68
RSR	14	1.30±0.63	11	0.36±1.12	25	0.88±0.98
SP	20	1.70±1.01	15	1.72±1.17	35	1.71±1.07

The mean values of these variables for each profile were entered into a model in which the three locations were categorical variables ('Location') and Measurement Depth was assigned a dummy variable (Deep=1; Surface=0).

The ANOVA model for Θ was highly statistically significant with $p<0.0001$ ($F=32.6$ df 3/72), with the significance attributable to differences across locations ($p<0.0001$); Θ was not significantly related to measurement depth (i.e., within Location) ($p>0.25$). The pooled values of Θ by Location were 184.6°±70.7° for Ben, 81.1°±8.1° for RSR, and 118.5°±9.1° for SP (note the relative high variability for Ben).

The ANOVA model for a was marginally statistically significant ($p=0.04$; $F=2.91$ df 3/72), with the significance attributable to differences across locations ($p<0.02$); a derived from the model was not significantly related to measurement depth (i.e., within Location) ($p>0.6$). For both Θ and a Location-by-Measurement Depth interactions were not statistically significant ($p>0.05$). The pooled values of a by Location were 0.92±1.68 m for Ben, 0.88±0.98 m for RSR, and 1.71±1.07 m for SP. Were one to assume that the cable maintained a constant depth along its entire route as an engineering specification, then the mean cable depth, a, pooled across all 76 profiles was 1.27 m (standard deviation, sd=1.25 m; se=0.14 m).

Current

Trans Bay Cable kindly provided daily average load±sd expressed in MW, and assuming a constant voltage of ±200 kV, current was calculated as watts/($4*10^5$ volts). For TBC, the daily means over the eight measurement days (Table 2-2) averaged 722±95 A std dev and the modeled values averaged 823±208 A std dev, resulting in a difference of 101 A with a paired two-tailed t-test with $p>0.10$ (t=1.71, df=7). The eight paired mean values yielded a Spearman correlation coefficient of 0.60 ($p=0.12$) (and a Pearson value of 0.62, $p=0.10$) (Figure 2-8, which includes the least-squares regression line).

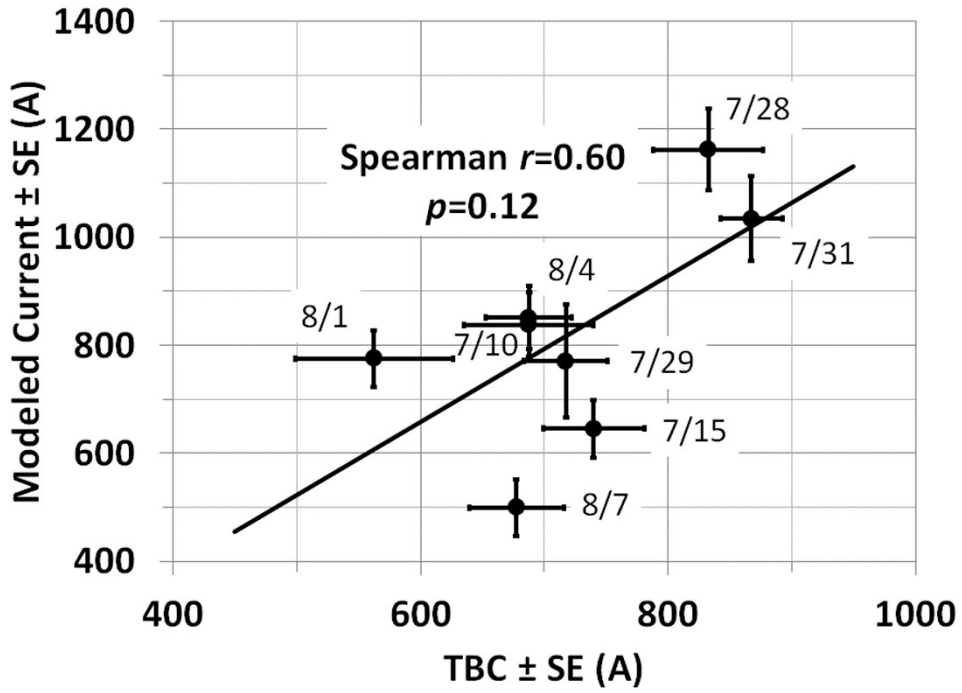

Figure 2-8 Average modeled current versus average current provided by TBC for each of the eight days for which data are reported.

The least-square regression line is shown. Note SE for TBC is based on the assumption that the variance provided was based on 24 hourly samples; for the survey described here, SE is based on number of survey lines for each day.

Discussion

The mean values of twist angle, Θ, cable depth, a, and load current, I, derived from the regressions appear to bear a consistency with what one could expect from direct observation of these parameters. The values derived from regressing any single profile would not be expected to be a reliable estimate of the cable's characteristics, but the objective of growing the sample size as large as possible is to have errors even out on both the positive and negative side.

The ambient DC magnetic field detected by the magnetometers included all sources of DC magnetic fields and all perturbations of the background magnetic field, whether caused by large objects, other electrical activity, or by field variations associated with ferromagnetic deposits in the upper earth's crust. Thus, while a distinct pattern of an anomaly associated with the cable could be visually discernible, we cannot assume the field pattern was pristine, that is, due to only the cable and the geomagnetic field posted on the NOAA website for the location of interest. The modeling also accepted profiles whose angle relative to the cable's direction were 90°±12.8°, a decision that introduces an error of up to 2.5% in the calculated cumulative distance

from the first measurement point of a survey line's field profile, although the error was typically much less (data not shown). The trade-off for enforcing a tighter tolerance would have been a loss of data.

Detectability of Anomalies

The magnetometers appeared to be exquisitely sensitive to the DC magnetic field environment in all locations surveyed. The manufacturer specifies a nominal resolution of 3 nT, and that sensitivity was abundantly apparent as they detected anomalies from the cable as small as about 50 nT. Detection of cable-associated anomalies was clearly handicapped by the presence of bridge structures. At the BB, only 2 of 40 (20 Deep, 20 Surface) profiles had detectable anomalies, which manifested as 'blips' on a profile mostly obscured by the bridge and other unidentified objects. In addition, the magnetometers recorded evidence of the activity of the Bay Area Rapid Transit (BART) system - which operates at 1,000 V DC - at the edge of various BB profiles although distant from the cable crossing of the profiles.

At Ben, 7 of 24 (29.2%) Deep profiles and 9 of 24 (37.5%) Surface profiles could be analyzed in the regression model, all but one of these (a surface profile) on the southwest side of the bridge. Anomalies for the profiles immediately adjacent to the bridge and all those northeast (save one) were not visually resolvable. The most obvious explanation for the latter would concern unidentified submerged objects with magnetic properties located on the northeast side of the bridge.

RSR provided a very distinct pattern of readable as opposed to non-readable anomalies. A total of 20 profiles were measured for both Deep and Surface, 10 south of the bridge and 10 to the north. The three profiles immediately to the north and south were not readable, although one could see a distortion of the anomaly in several of these. For the Deep profiles all of the others, 14 of 20 (70%) were regressed, and 11 of 20 (55%) Surface profiles were regressed.

No bridges were located in SP, affording an opportunity to measure in relatively 'open water' resulting in resolving nearly all of the Deep profiles (20/21, 95.2%) and the majority of the Surface profiles (15/21, 71.4%). There may have been other objects in SP that perturbed the Surface measurements, they having weaker fields from the cable than Deep measurements, while the fields at the deeper measurement locations may have surmounted any perturbances.

Compared to RSR and SP, Ben had the greatest variability in Θ and a, (Tables 2-4 and 2-5) and the regressed profiles at Ben-S did not produce estimates of min-max distances consistent with the values based on the measurements (although Ben-D did) (Figure 2-8). One plausible reason for the large variability is that the estimate of Θ (184.6°±70.7°) for Ben-S includes 200°, which has a much less distinct anomaly pattern than the more typical 'whiplash' shape with a distinct structure lending it comparatively more amenable to a precise regression. The imprecision of estimating min-max differences for Ben-S was not related entirely to a lack of sensitivity attributable to having the lowest anomaly of all eight groups (93.5±42.4 nT). For RSR-S, with nearly the same average anomaly (second lowest with 95.7±13.4 nT), but with a 'whiplash' field contour, the estimated min-max differences were consistent with the measured values. These factors are illustrated in Figure 2-9 with curves based on idealized calculations (as in Figure 2-4). They show the unimodal pattern of the anomaly with Θ=200° (and Φ=-57°), characteristic of Ben-S along with the slightly more distinct shapes at 175° and 225°. By comparison, RSR-S had an estimated Θ of lesser variability of 81.1°±8.1° (with Φ=-53°), which produces more of the whiplash shape shown in Figure 2-9 that apparently resolves comparatively better in the regression exercise.

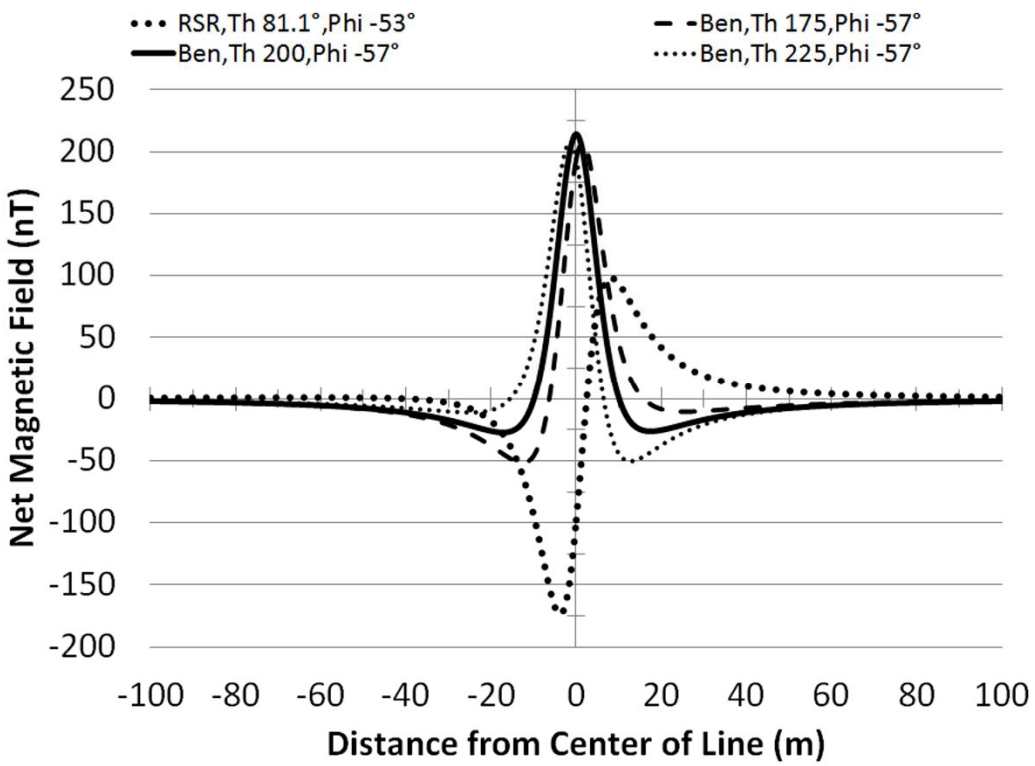

Figure 2-9 Variability of profile pattern structure.

An illustration of how the profile has a less distinct pattern for Θ and Φ in the Benicia-Martinez Bridge (Ben) data set centered on $\Theta \approx 200°$ (thick black line), compared to the more distinct 'whiplash' pattern for Θ and Φ in the Richmond San Rafael Bridge (RSR). The Ben curves for $\Theta=175°$ and $\Theta=225°$ illustrate transitional patterns with a more distinct structure than for $\Theta=225°$.

Anomaly

Regardless of these sources of error, the values of the parameters produced by the regression produced an excellent fit with the observed anomalies with their magnitudes practically identical. The regressions underestimated the distance between the minima and maxima by 6.3%, a difference that is not readily explained, but may be due to deviations in the cumulative distance from the first measurement point that were calculated from the LAT-LONG data, for example, due to ocean current, exact vessel heading, and an angle between the survey line and cable that was not exactly perpendicular. The slight underestimate of max-min distance in the model result is not considered of great importance by the investigators.

For a cable such as the TBC, the magnitude of the anomaly scales directly with current and decreases as the inverse square of the distance above the cable. However, there remains a dependency also on Θ and Φ. The 3-D contour charts in Figure 2-10 illustrate how the anomaly's magnitude decreases by a factor of 4 when the height, h, above the cable doubles (the contour retains the same shape with respect to Θ and Φ at both heights). The variability across Θ and Φ should be evident in the contours, with a max:min ratio of about 1.3.

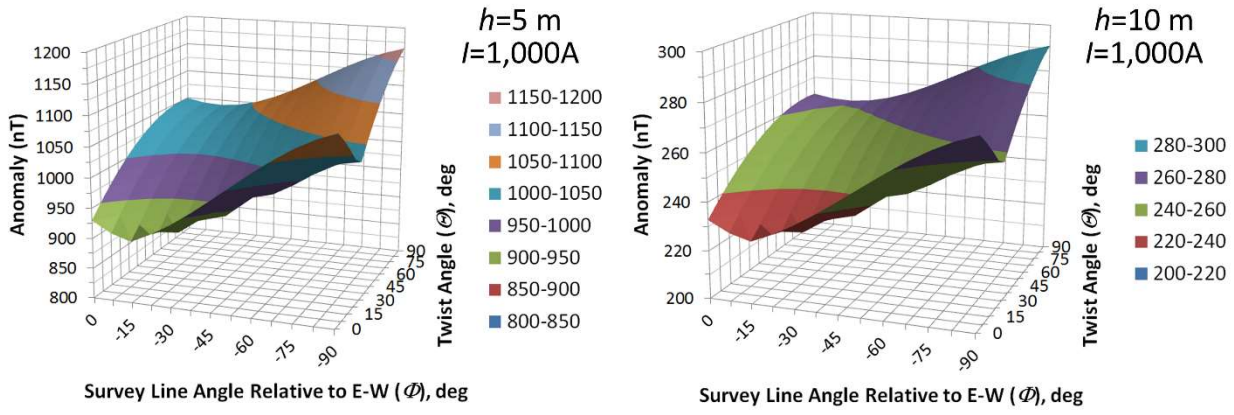

Figure 2-10 Sensitivity of the anomaly to height above the cable, as well as to Θ and Φ.

See text.

Twist Angle, Θ

At any location along its route, the cable's twist angle, Θ, has an effect on the magnitude of the anomaly associated with the load on the cable. For example, for a field profile 10 m above the cable loaded at 1,000 A, with survey line angle, Φ=-55° (similar to Φ at Ben and SP), the calculated anomaly can vary over a 14.3% range relative to the anomaly averaged over 360° (259 nT). Thus, to predict what the anomaly may be at any of the three locations, an accurate estimate of Θ is desirable. Despite the high variability of the estimate of Θ for Ben, the data suggest that the cable may twist gradually along its path between Pittsburg and San Francisco (Table 2-4). The high variability of the estimate of Θ for Ben may also be based on a comparatively less distinct field profile at the Ben location (Discussion above and Figure 2-9).

Cable Depth, *a*

Cable depth is a challenging parameter, because it represents only a portion of the vertical drop from the magnetometer to the cable itself, and the regression solves for total height with a the difference between height and ALT. For the surface measurements (N=35), the ratio of a to the average of ALT across each profile was 0.092±0.125, and for the deep measurements (N=41), the ratio was 0.177±0.138, a difference with p<0.01 (t=2.78, df=74). A reflection of the lability of the cable depth estimate as relates to measurement depth was that 8 of the 35 surface profiles had negative estimates of a, and only 2 of the 41 deep profiles had negative estimates. Of course, a negative value is implausible, representing the cable as above the water's bottom surface. The difference between the frequency of negative estimates in the surface and deep profiles was statistically significant (Fischer's exact test; p=0.0234). Understanding cable depth is important from the perspective of estimating anomalies. Using the example from above (1,000 A, 10 m height) the average anomaly over all possible values of Θ in 7.5° increments and Φ from 0° to -90° in 7.5° increments is 259 nT, with a slope of -52 nT per meter increment above the cable. Thus, with regard to calculating an anomaly at a particular point, errors in estimating a can be at least as sizable as errors associated with estimating Θ.

Current

Load currents were derived from magnetic field profiles measured during daytime hours on eight days in July and August 2014. The averages of these derived values for each day were compared to 24-hour average loads for the same days furnished by TBC. Thus, the two data sets, though

plotted against each other (Figure 2-8), were based on different time frames. However, the two sets otherwise had mean currents that were similar in magnitude and positively correlated with one another, though not with statistical significance ($p \approx 0.1$).

Of greater concern is that for 20 of the 76 profiles reported, the derived currents exceeded the nominal load rating of the line (1,000 A). A portion, if not all, of these exceedances can be attributed to variability inherent in the regression model. It is not known to the investigators whether some of these were due to periods of the day in which TBC was asked by the system operator to increase load beyond the rated level to satisfy demand for electricity.

Conclusion

The magnetometer used in the suey of magnetic fields in the San Francisco Bay faithfully recorded the ambient DC magnetic fields in its pathway. Otherwise, the regressions of the visible anomalies could not have possibly produced the matches as exemplified in Figure 2-5. This study has demonstrated that the regression formulas applied to the measured profiles based on the fundamental principle of the Biot-Savart law and the vectorial summation of cable and geomagnetic fields in rectangular coordinates provide estimates of cable characteristics consistent with plausible expectations. Nonetheless, various factors contribute to variability inherent in such an effort, particularly uncontrollable sources of field perturbations that do not lend themselves to modeling, and remain empirical observations. Whether magnetic field perturbations of a large magnitude from fixed structures and objects clustered in individual locations contribute to behavioral modifications in fish, as opposed to relatively small anomalies on the order of <1,000 nT continuously present along an 85 km long DC cable route is the subject of ongoing and possibly future research. Regardless, the methods described in this paper should be applicable to other buried HVDC cables. However, they would not apply to buried alternating current (AC) power cables for which modeling would be more complex.

3 CHINOOK SALMON AND GREEN STURGEON MIGRATE THROUGH SAN FRANCISCO ESTUARY DESPITE LARGE DISTORTIONS IN THE LOCAL MAGNETIC FIELD PRODUCED BY BRIDGES

Introduction

Empirical evidence exists that marine animals perceive and orient to local distortions in the earth's main geomagnetic field. Scalloped hammerhead sharks have been shown to use these fields to guide their diurnal migrations from a seamount to and from nighttime feeding grounds. [15] This ability to orient to local maxima and minima can be described as geomagnetic topotaxis. The prefix topo describes the relationship of the animal's trajectory to topography, defined in the dictionary as "the configuration of a surface including its relief and position of its natural…features". [16] The suffix taxis indicates that an animal is attracted to a stimulus. In this instance, the animal actively tracks geomagnetic ridges and valleys, features of relief in a surface of geomagnetic field intensities.

Seamounts are of volcanic origin with a dipole magnetic field present at the cone and strong and weak magnetic fields emanating from the lava flows that extend away in all directions. A local distortion is produced by single-domain particles of magnetite that become aligned with the earth's main field at the time of a volcanic eruption as the molten lava hardens. If eruptions are separated greatly in geological time, the next eruption may occur after the earth's main field has reversed. This results in the particles becoming fixed in the reverse direction as the basalt cools and hardens. The fields from these magnetic particles, which are aligned either parallel or antiparallel to the current polarity of the main field, produce magnetic maxima and minima ("ridges" and "valleys" in a topographic sense) leading away from the volcanic source. The migratory movements of hammerhead sharks coincide with these magnetic ridges and valleys leading away from the seamount. [15]

Molten basalt is extruded from spreading centers along a north-south axis in the middle of the oceans to form the seafloor and continental crust of the earth. Magnetite particles within the molten basalt align to the current polarity of the earth's field as the basalt cools and hardens. The periodical pole reversals result in alternating strong and weakly magnetized sections of crust in a north-south orientation, depending upon whether the magnetite is aligned parallel or antiparallel to the prevailing orientation of the earth's main field. Evidence exists that baleen whales strand where rotation of an oceanic plate results in weakly magnetized sections intersecting the western coastline of Great Britain [17] and eastern coastline of North America. [18]

The electromagnetic fields (EMF) generated by the cables that carry electric power from hydrokinetic energy generating sources to shore-based power stations may likewise produce local distortions in the earth's main field. Concern exists that animals that migrate along the continental shelves might orient to the EMF from the cables, and move either inshore or offshore, away from their normal paths. Would the sharks that migrate northward during summer and southward during winter be misdirected by offshore cables as they migrate along the eastern coast of North America? Similarly, would the gray whales that migrate back and forth between central California and the Baja Peninsula be affected by the EMF of an offshore cable?

For this reason, we have studied the effect of the Trans Bay Cable (TBC), an 85-km long high voltage, direct current transmission line leading from Pittsburg, CA to San Francisco, CA on fishes migrating through the San Francisco Estuary (Figure 2-1). These are Chinook salmon smolts (*Oncorhynchus tshawytscha*) [5, 6] that emigrate downstream through the San Francisco Estuary to the Pacific Ocean and adult green sturgeon (*Acipenser medirostris*), which immigrate upstream through the San Francisco Estuary to their spawning habitat in the upper Sacramento River [3] [19] and subsequently, back down to the ocean after spawning occurs. Studies have established that species within the salmonid family use the natural ambient magnetic (or electric) fields to guide their movements during migration or foraging behaviors [8-11]. Anatomical studies have revealed that the sturgeons have electroreceptors, and hence are capable of using similar fields to provide guidance during migration [20].

Previously, we described the effect of the TBC's load current on the local magnetic field. [21] Its fields were measured while traversing the cable roughly perpendicular to its path at varying heights above the sea floor. Gradiometer surveys were conducted at four sites: 1) San Francisco-Oakland Bay Bridge (BB), 2) Richmond-San Rafael Bridge (RSR), 3) Benicia-Martinez Bridge (Ben), and 4) San Pablo Bay (SP). Seventy eight of 167 survey lines at these sites yielded profiles indicating the cable's presence. The anomalies produced by the TBC were compared to those predicted from a direct current cable with formulae using the physical properties of the cable, its depth in the ground, the current passing through it, and the height the magnetometer was towed above the seafloor. A strong concordance was found between the empirical and calculated anomalies. This knowledge permits researchers to estimate the magnitude of the fields from DC current sources, given they have information about the conductor, its depth, and its load, without having to conduct exhaustive gradiometer surveys in the future. (Magnetic fields from AC cables can only be crudely approximated with similar methods.)

In this paper, we compare the fields emitted by TBC to the anomalies in the geomagnetic field created by the three large bridges running perpendicular to the migration routes of these species. The strengths of the anomalies from the bridges exceed those of the cable by a magnitude of a power of ten or greater. We report that these strong anomalies from the bridges do not present an insurmountable barrier to the migration movements of salmon and sturgeon migrating through the San Francisco Estuary. In a future paper(s), we will examine the effect of the cable on the migratory path of Chinook salmon and green sturgeon.

Methods

Magnetic field surveys were conducted in four locations of the San Francisco Bay between July 10th and August 8th, 2014 (Figure 2-1). A cross-bay array of acoustic biotelemetry receivers existed at each site, the San Francisco-Oakland Bay Bridge, the Richmond-San Rafael Bridge, and the Benicia-Martinez Bridge, as well as a non-bridge location in the San Pablo Bay. Surveys were performed with a transverse gradiometer (G-882 TVG, Geometrics, Inc., San Jose, CA) (Figure 3-1). This device is equipped with two cesium vapor gradiometer 'fish' separated by 1.5 m on a frame with stabilizer weights and fins. The dual cesium sensors are synchronized to 1 ms sampling with sensitivities up to 0.004 nT/√Hz RMS or approximately 0.01 nT peak to peak at

10 Hz. A depth sensor (depth under the water surface, 0.5% accuracy) and an echo-sounder altimeter (height above the sea floor, 1% resolution) attached to the frame provided positional information to the operators. Data was transmitted through the reinforced tow line to our onboard computer (Toughbook, Panasonic), which was interfaced with a Trimble GeoExplorer XT Global Positioning System (GPS) with Hurricane LI antenna (Trimble Navigation Limited, Sunnyvale, CA) for display of the magnetic intensity measurements at different positions with sub-meter accuracy (after post-processing). The gradiometer was carried on a wooden platform, lowered into the water with an A-frame, and towed along survey lines pre-mapped with MagLog magnetic data acquisition software (Geometrics, Inc.). The MagLog display on the computer provided a graphic representation of the vessel's location in relation to the pre-mapped survey lines, and this was used by the helmsperson to steer the boat very precisely along the length of the survey line.

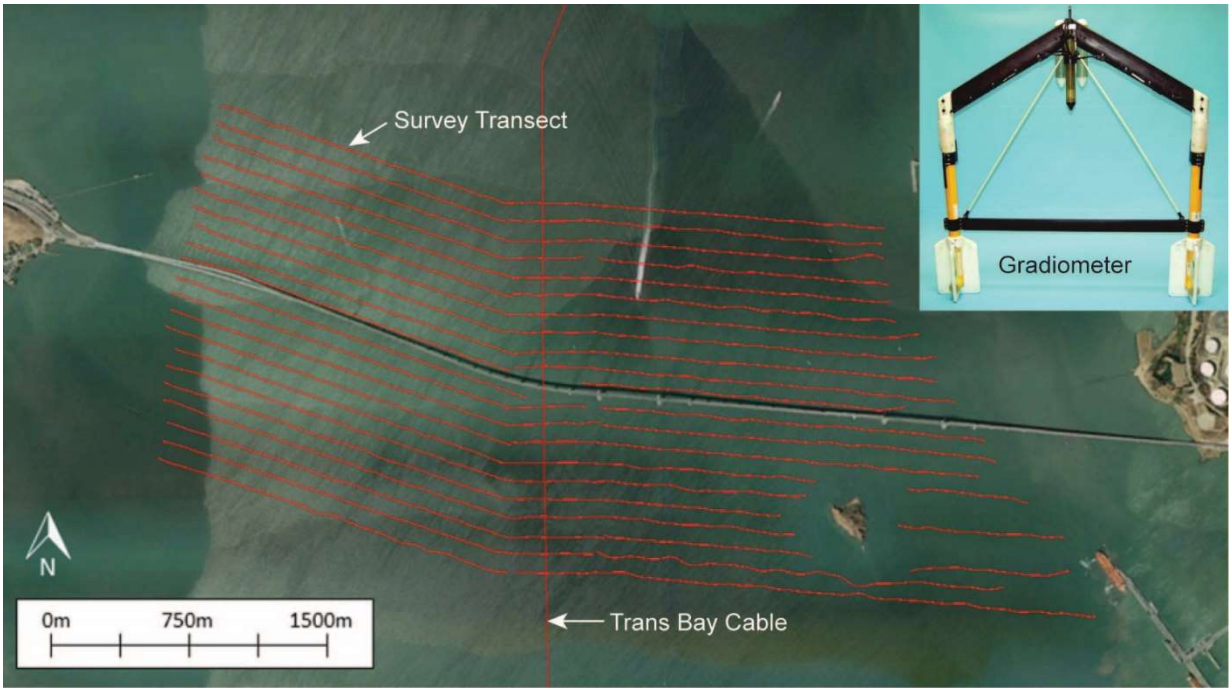

Figure 3-1 Magnetic survey transects conducted at Richmond Bridge.

The survey transects (see horizontal red lines) extended one kilometer to either side of bridge. The path of the Trans Bay Cable (vertical red line) passes under the bridge in a north-south orientation. Insert: transverse gradiometer (G-882 TVG, Geometrics, Inc, San Jose, California) featuring two magnetometers mounted side by side 1.5 m apart (Photo: Geometrics).

Two types of survey lines were conducted. Firstly, the gradiometer was towed parallel to the acoustic arrays. These lines extended along the entire span of the bridge as far towards the banks

as possible and at least 1 km outwards from the fish detection array in San Pablo Bay. Transect lines started as close to the bridge/array as possible on each side and were repeated every 100 m away from the bridge/array up to 1 km (Figure 3-2). The purpose of these survey tracts was to verify the model of the magnetic fields produced by the cable (see Kavet et al. for details, [21]) and to provide data needed to create a local magnetic field map and a local magnetic field gradient map over the detection range of the fish detecting monitors. Secondly, the gradiometer was towed perpendicular to the bridges out to 1 km on both sides of each bridge. At least three of these transects were conducted at each bridge site. The purpose of these transects was to measure the magnetic field distortion created by the bridges. All survey tracts were conducted close to the surface (0 - 3 m below the water surface) and at greater depth in deeper locations (maximum of 12 m off the channel bottom). We conductecd tows at these two depths in order to ensure that we sampled both the upper and lower magnetic field profiles in the water channel.

After the survey, the survey data was post-processed and mapped using MagPick gradiometer data processing software (Geometrics, Inc., http://sourceforge.net/projects/magpick/). [22] Post-processing included the following: 1) differentially correcting the GPS points to get sub-meter accuracy on survey locations using Trimble GPS Pathfinder Office software (Trimble Navigation Ltd.), 2) correcting for tidal stage based on tidal stage data downloaded from the nearest port stations operated by the National Oceanic and Atmospheric Administration, NOAA, 3) correcting for fluctuations in the Earth's magnetic field by subtracting the magnetic field measures recorded at the Jasper Ridge Biological Preserve base station from our field measures, and 4) removing DC offset between the two magnetometers. After post-processing was complete, two types of maps were constructed for each survey area using the survey lines that run parallel to the bridges/arrays. The first is a total local magnetic field map that illustrates the anomalies present in the local magnetic field, calculated as the average magnetic field measured by the two magnetometers minus the Earth's magnetic field. The second is a gradient map (also called a quasi-analytic signal map), which depicts the rate of change in the local magnetic field anomalies in nT/m. The magnitude of the quasi-analytic field was calculated using 1) the transverse component of the gradient vector of the local magnetic field using the difference of the two magnetometers divided by their 1.5 m separation, 2) the longitudinal component of the gradient vector using the average of the two magnetometers and the data collected along the

survey line, and 3) the estimated vertical derivative of the gradient vector (see 15 for details). These maps were created for the surface and deep tows at each survey location, but only the Richmond Bridge surface maps are shown here as illustrations. Graphs of the data recorded by these individual profile lines were also produced, with distance along the survey line extending from east to west in meters on the abscissa and the measured magnetic field in nanotelsa (nT) on the ordinate. The strength of local magnetic anomalies, such as those produced by the cable or the bridges, were quantified by taking the difference between the maxima and minima magnetic field values measured by the gradiometer along its survey route as it passed perpendicular to these objects of interest.

Records of fish movement were utilized from previous biotelemetry studies carried out both before and after the Trans Bay Cable was installed in the San Francisco Estuary. In these studies, Chinook salmon smolts were tagged with uniquely coded ultrasonic transmitters and detected throughout the San Francisco Bay as they migrated to the Pacific Ocean by receivers attached to bridges or anchored on the channel bottom. The majority of Chinook salmon smolts used in this study were tagged and tracked through the bay as part of a study to determine the reach-specific rates of movement and survival funded by CALFED and their movements relative to dredge removal and deposition sites funded by the United States Army Corps of Engineers. [5, 6] Coded ultrasonic transmitters were also placed on adult green sturgeon captured throughout the estuary and northern California coast to understand the factors governing their upstream spawning migration to the headwaters of the Sacramento River, primarily funded by the California Department of Fish and Wildlife and United States Bureau of Reclamation. [3, 19]

Results

Magnetic Anomaly from Cable

The DC current passing through the Trans Bay Cable, generated for local demand (load), produces a magnetic field that adds as a vector to the earth's natural field. This vector addition leads to the appearance of a disturbance in the local background field. The localized anomaly in the total field from the TBC was clearly recorded by the gradiometer during the surveys. It is apparent from the thin line with dark blue and red points with a vertical orientation on the map of the total field intensities at the Richmond Bridge (Figure 3-2). These were produced as the

magnetometer passed over the cable from east to west at 100 m distance intervals away from the bridge on either side. The surface anomaly is apparent on the map as hue change from blue green to red, equivalent to a difference from 238 nT to slightly over 292 nT on the color bar -- a magnitude of 54 nT using the color bar to estimate the anomaly. The field distortion produced by the cable is also apparent in the map of the geomagnetic gradient, termed quasi-analytic signal (Figure 3-3). The geomagnetic gradients recorded as the gradiometer passed over the cable at 100 m distance intervals are apparent from a change in color from purple to yellow, a difference from a fraction of one nT/m to four nT/m. The TBC anomalies produce minute alterations in the earth's main field.

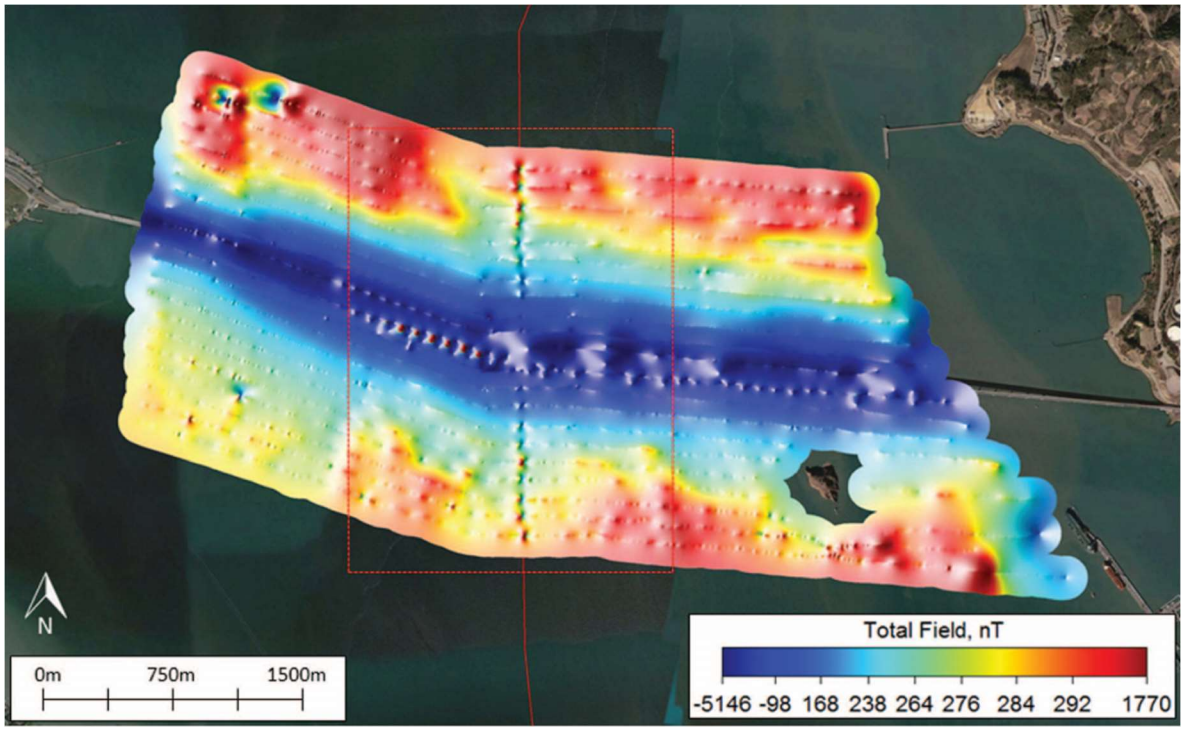

Figure 3-2 The local magnetic field anomalies existing around the Trans Bay Cable and Richmond Bridge.

Note that the anomaly in the field produced by the cable is evident in the dark blue and red points along the line indicating the path of the cable that passes through the bridge along a north-south axis. The color scale uses non-linear color mapping based on the data distribution. Using this color equalization technique, each color occupies the same area on screen as any other color, ultimately increasing map resolution and visualization of smaller magnetic anomalies.

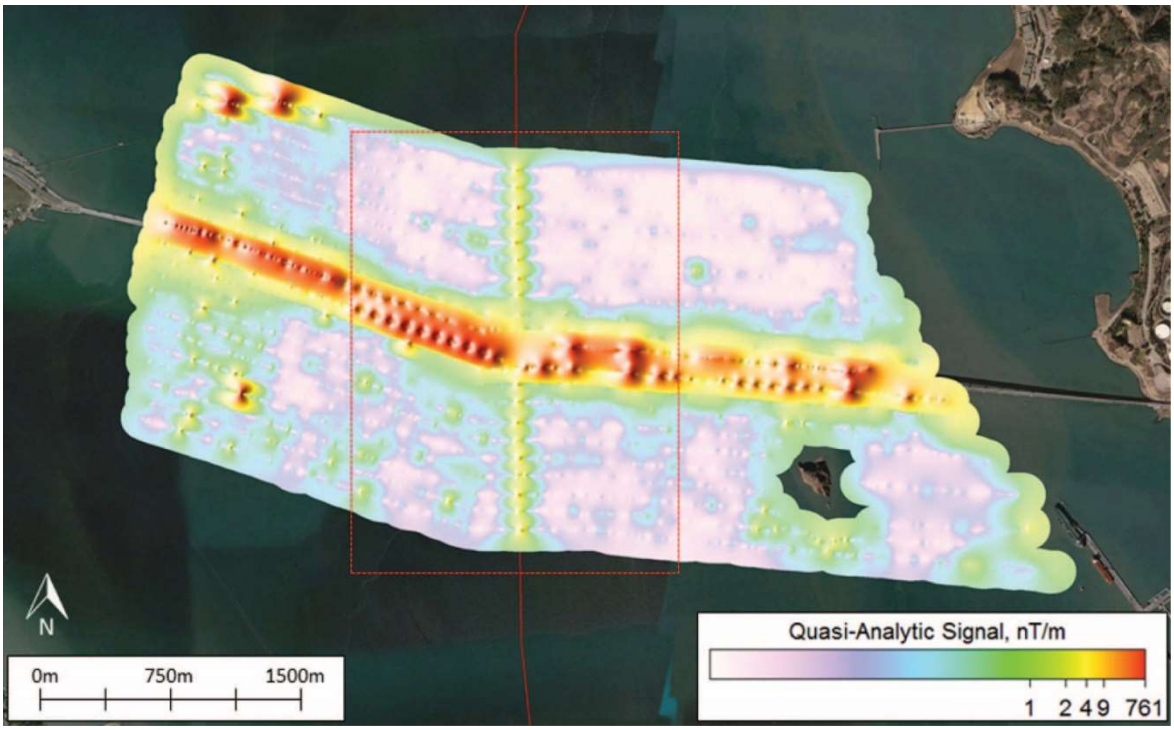

Figure 3-3 The gradient map of local magnetic fields existing around the Trans Bay Cable and Richmond Bridge.

This quasi-analytic signal map illustrates the rate of change in local magnetic field anomalies, denoted as nT/m. Note that the rate of change in the local magnetic fields associated with the bridge is much greater than near the cable, and the distortion in the field extends farther from the bridge than the cable.

The distortion in the main field by the EMF from the cable was also distinguishable in plots of the magnetic field anomaly as a function of distance traveled from east to west along the survey routes perpendicular to the cable. Profiles of magnetic intensity are shown as the gradiometer was towed across the TBC ca. 900 m north of Richmond Bridge both at the surface and sub-surface (Figure 3-4). The strength of the magnetic signal at the surface decreases from nearly 300 nT to a minimum of 226 nT, then increases to a maximum of 320 nT, before returning again to a relatively steady state at 290 nT, all over a distance of 150 m. The overall magnitude of the anomaly measured during this surface transect was 94 nT. As one might expect, the anomaly recorded when the gradiometer was towed closer to the channel bottom along the same transect was greater than that recorded at the surface. The signal strength decreased from 290 nT to a minimum of 206 nT, then increased to 455 nT, before dropping to its relatively steady state of 280 nT, giving an overall anomaly of 249 nT recorded over a distance of 150 m. The mean

magnitudes of cable-associated anomalies measured during surface tows near the Benicia and Richmond Bridges and San Pablo Bay ranged from 93.5 to 117.0 nT, whereas the magnitude of the anomalies recorded during sub-surface tows at the same bridges varied from 235.6 to 518.0 nT (Table 3-1). The anomalies from the cable recorded during the sub-surface tows were significantly greater than those from the surface tows (Kruskal-Wallis Test, $p<0.0001$), as the field from the TBC attenuated substantially from a meter over the bottom near the buried cable to a meter near the surface.

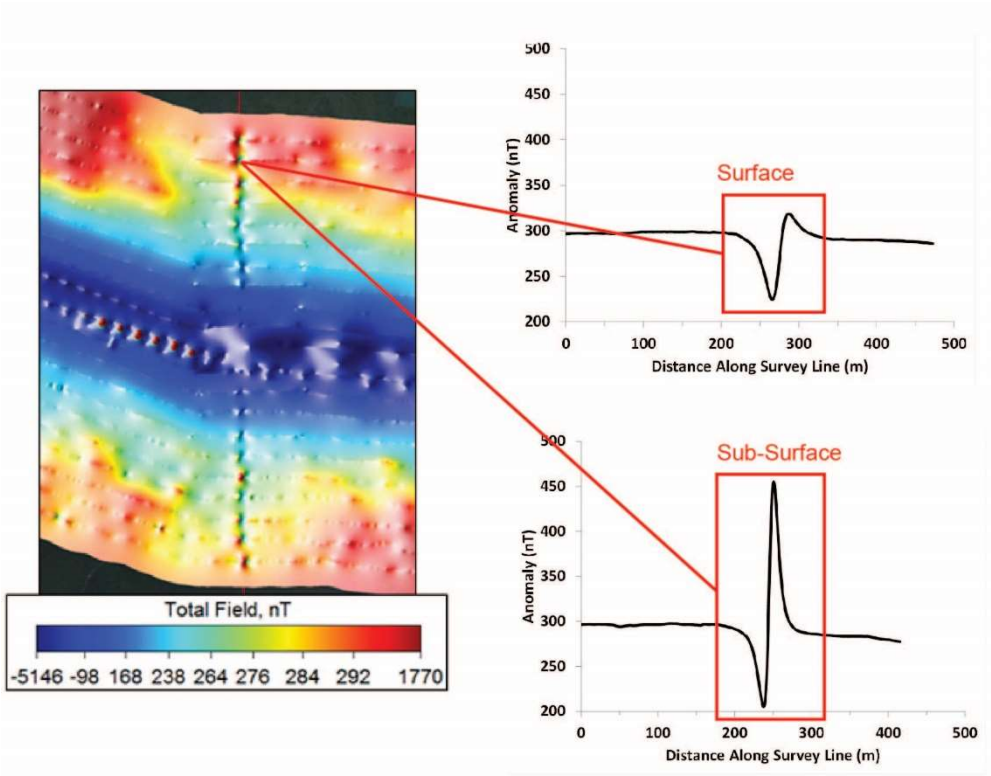

Figure 3-4 The magnetic anomaly induced by electrical current passing through the Trans Bay Cable.

Profile plots of the cable's measured magnetic anomaly are illustrated for both surface and deep tows along survey transects far away from the bridge. The anomaly is shown as the gradiometer was towed from east to west over the cable along transects orientated parallel to the bridge and perpendicular to the path of the cable. The anomaly recorded at the surface was 94 nT while the anomaly near the bottom was 245 nT. The increase in magnetic intensity in the latter profile was due to the gradiometer's increased proximity to the EMF-producing cable. The anomaly occurs over a distance of 80 meters, and consists of a negative and positive increment to the main field.

Table 3-1 Summary of magnetic field anomalies associated with the Trans Bay Cable (TBC) and bridges in the San Francisco Estuary.

The local magnetic fields (in nanotesla, nT) of the bridges and cable were measured with both surface and deep tows during transects that ran perpendicular to the object of measure. The cable was surveyed at bridge site locations as well as a non-bridge location in San Pablo Bay. Cable data is only presented from transects where the cable anomaly was clearly identifiable. Measurements from the two magnetometers were averaged for this study.

		Benicia Bridge		Richmond Bridge		Bay Bridge		San Pablo Bay
		TBC	Bridge	TBC	Bridge	TBC	Bridge	TBC
Surface	Transects (N)	9	2	11	4	0	5	15
	Mean	93.5	2507	95.7	2236	--	2732	117.0
	SD	42.4	490	13.4	1241	--	2184	22.1
	Median	76.4	2506	93.9	2374	--	1479	115.8
	Min	54.2	2160	72.9	728	--	901	68.5
	Max	192.9	2853	122.2	3468	--	5923	151.1
Deep	Transects (N)	7	1	14	3	2	4	20
	Mean	235.6	--	268.5	1142	518.0	4168	300.6
	SD	84.4	--	49.4	737	241.8	1997	130.5
	Median	207.9	3442	262.4	726	518.0	4363	286.1
	Min	139.8	--	197.6	707	347.0	1847	144.9
	Max	359.9	--	380.5	1993	689.0	6100	661.3

Magnetic Anomalies from Bridges

The magnetic anomalies associated with the bridges differed from the cable anomaly in form, magnitude, depth distribution, and geographical extent. Let us first compare the anomaly from the Trans Bay Cable to that of the Richmond Bridge. The movement of electrons in one direction through one cable and their movement in the opposite direction on the adjacent cable created a dipole magnetic field that subtracted from the earth's main field to the east of the cable and added to the field to the west of the cable at the Richmond Bridge. The waveform on the magnetometer records was not symmetrical with the negative excursion being smaller than the positive excursion in the case illustrated. This was due to the vectoral addition of the local main field and the dipolar field of the cable, and reinforcement of the field on one side and some cancelation on the other side. The structure of the anomaly from the bridge is more complex. The ferromagnetic materials within the bridge abutments, which are likely concrete with iron bars, concentrate the flux lines from the earth's field leading to a deficit between the abutments. This is apparent in the scalloped pattern of alternating positive and negative peaks on the record of the total field when the boat was driven parallel to the bridge (see Figure 3-6). This pattern differed from the single negative peak on the record when the magnetometer was towed under the bridge (see Figure 3-6). The magnetometer passed within 25 m of abutments during the former transect and 50 m during the latter. For this reason, the positive anomalies from the abutments were present on the record from survey line along the length of the bridge and not on the line underneath the bridge, in which the boat was 50 m from the closest abutments. The latter survey line was farther from the abutments, and for this reason the anomaly was more negative than for transect parallel to the bridge. In conclusion, a large object with ferromagnetic materials, such as the Richmond Bridge, thus rearranges the magnetic flux lines from the earth's field, which would be relatively uniform in the bridge's absence.

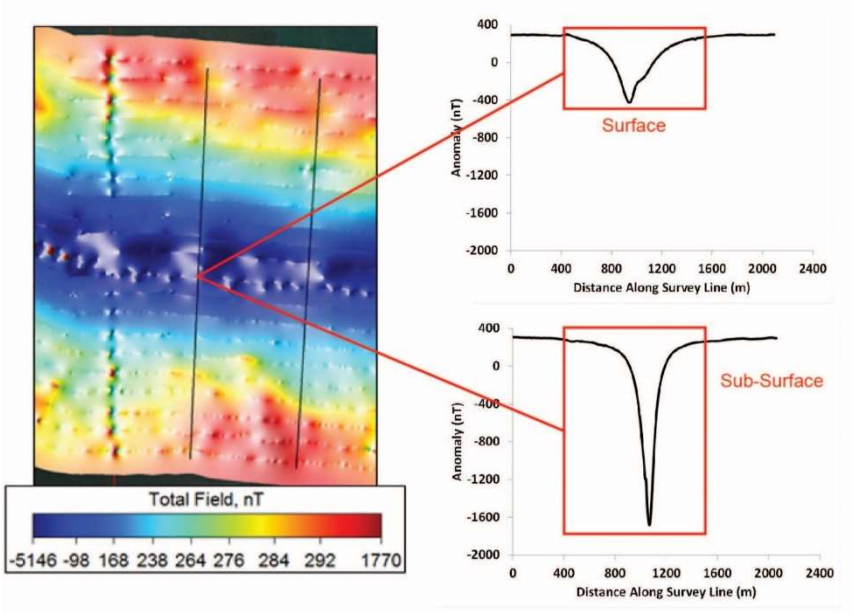

Figure 3-5. The magnetic anomaly produced by the Richmond Bridge as measured by perpendicular survey lines.

Profile plots for surface and deep tows are illustrated along transects (black vertical lines) travelling perpendicular to the bridge. Note that the surface anomaly from the bridge is 728 nT and sub-surface anomaly is 2,000 nT, exceeding that of the cable in magnitude by a factors of 7.7 and 8.2, respectively. The anomaly occurs over a distance of 1,200 m, and does not consist of a positive and negative excursion but simply a negative excursion.

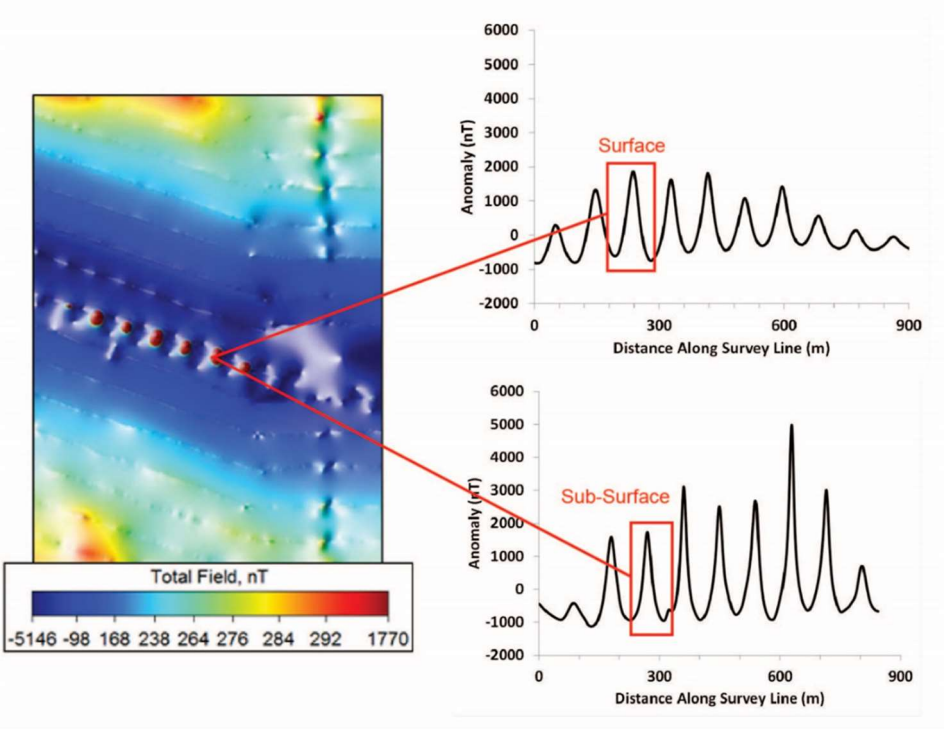

Figure 3-6. The magnetic anomaly produced by the Richmond Bridge as measured by parallel survey lines.

Profile plots for surface and deep tows are shown for a survey transect located parallel to Richmond Bridge, approximately 50 m south of the bridge. Successive maxima and minima along the profile are separated by a distance of 100 m, the approximate distance between bridge supports. These observations indicate that the supports are also a strong source of anomalies, adding to the field at each structure, and subtracting from the between each structure.

The bridges produce larger anomalies in the total field than those produced by electricity passing through the Trans Bay Cable to San Francisco. The difference in magnitude of the anomalies from these two sources of EMF was strikingly apparent both by visual inspection of the total field and gradient maps as well as by comparisons of the anomalies measured from the plots of magnetic intensity from survey transects orientated perpendicular to the cable and bridge. For instance, anomaly in the total field shown on the map varied from red to dark blue on the color scale, indicating variation on the order 1,770 to -5,146 nT (Figure 3-2). The anomaly in the quasi-analytic signal varied from the color purple to red on the color scale, a gradient of less than one to 761 nT (Figure 3-3). These values greatly exceeded those apparent in the visual inspection of the cable maps. Furthermore, the magnitude of anomaly produced by the Richmond Bridge at the surface was 700 nT, decreasing from 300 nT to -400 nT before rising the same level; whereas the anomaly measured near the t the bottom was 2,000 nT, decreasing from

350 nT to -1,700 nT before rising to the same level (Figure 3-5). The surface anomaly in the total field measured at the bridge was 7.5 greater than the anomaly measured at the cable during the survey track located 900 m north of the bridge (Figure 3-4); the sub-surface anomaly was eight times that of the anomaly at the cable. The mean measured strength of the surface magnetic anomalies created by the three bridges of 1672.0 nT was roughly 24 times that mean strength of 70.9 nT to the anomalies produced by the TBC. The mean strength of the sub-surface anomalies of the Richmond and Bay Bridges of 2655 nT exceeded the mean anomaly of 330.6 nT of the cable near the three bridges and San Pablo Bay was less, a factor of 8.0, but still substantial.

Unlike the cable anomalies, those from the bridges varied with depth at different bridges. While the negative excursion recorded on the sub-surface transect was greater than that recorded on the surface transect at the Richmond Bridge, this was not the case at the other bridges. At the Benicia and Bay Bridges, the anomalies from deep tows were less than those from surface tows. There was no significant difference in the magnitude of the negative excursions when the surface transects, on which the anomaly of the bridge was apparent, were compared to the sub-surface transects with distinguishable bridge anomalies (Kruskal-Wallis Test, $p<0.05$). These differences likely stem from variation in the construction materials of the bridge span and supports, the height of the bridge span over the water surface at the perpendicular crossing, and the volume of traffic occurring on the bridge at the time.

Finally, the bridges altered the earth's field over a greater geographic extent than the Trans Bay Cable. For example, the lateral width of the anomaly from the cable sampled near Richmond Bridge was roughly 150 m (Figure 3-2), whereas the width of the anomaly from Richmond Bridge extended outward over total distances of 1200 m (Figure 3-5). This lateral width from the bridge anomaly exceeded that of the cable by nearly an order of magnitude.

The large anomalies produced by the ferromagnetic properties of the bridges often masked the anomalies of the Trans Bay Cable. The anomaly in the total field produced by the cable could not be discriminated from the larger anomaly recorded to a distance of 300 m north and 200 m south of the Richmond Bridge (see the dark blue color on Figures 3-2, 3-4 thru 3-6). The

'signature' of the cable was not apparent on the four nearest transects parallel to the bridge on the north side and three transects on the south side. The anomaly in the magnetic gradient of the bridge masked that of the cable to a distance of 100 m north and south of the Richmond Bridge (see red signal in Figure 3-3). At the Bay Bridge, only two of 20 surface and 20 sub-surface surveys of total field revealed the effect of the Trans Bay Cable.

Passage of Migratory Fishes through Bridge Magnetic Anomalies

The strong magnetic anomalies produced by the bridges along the migration route of Chinook salmon smolts and adult green sturgeon do not appear to present a major barrier to migration movements in the San Francisco Estuary. Many of the tagged Chinook salmon smolts were detected near the Richmond Bridge and later when they reached the Golden Gate Bridge on their migration to the sea. A total of 1025 smolts with ultrasonic beacons placed on them from 2007-2011 were detected passing under the Benicia Bridge and entering San Francisco Bay (Table 3-2). Of this total, 573 (56%) were detected as they passed near to Richmond Bridge. A total of 457 (45%) reached Golden Gate Bridge at the mouth of the bay. Hence, a little less than half did not stop their outward migration upon encountering the strong anomaly at Richmond Bridge. We do not know the fate of the 452 smolts, or 44%, that did not reach Richmond Bridge after passing under Benicia Bridge as well as the fate of the 116, or 20%, that did not pass from the latter to Golden Gate Bridge.

Table 3-2 Passage of Chinook salmon smolts and adult green sturgeon through the magnetic anomalies produced by the Richmond, Benicia, and Golden Gate Bridges.

Data represents the number of individual fish detected at each bridge in each year as well as the percentage of total fish detected at the first array for subsequent locations along each migration route.

	Chinook Salmon (Outbound Migrations)			Green Sturgeon (Outbound Migrations)			Green Sturgeon (Inbound Migrations)		
Year	**Benicia Bridge (N)**	**Richmond Bridge N (%)**	**Golden Gate N (%)**	**Benicia Bridge (N)**	**Richmond Bridge N (%)**	**Golden Gate N (%)**	**Golden Gate (N)**	**Richmond Bridge N (%)**	**Benicia Bridge N (%)**
2007	32	19 (59%)	25 (78%)	5	3 (60%)	4 (80%)	6	5 (83%)	6 (100%)
2008	143	61 (43%)	61 (43%)	7	5 (71%)	7 (100%)	4	3 (75%)	4 (100%)
2009	375	201 (54%)	150 (40%)	12	12 (100%)	12 (100%)	5	5 (100%)	5 (100%)
2010	332	215 (65%)	165 (50%)	36	34 (94%)	33 (92%)	9	9 (100%)	8 (89%)
2011	143	77 (54%)	56 (39%)	19	19 (100%)	19 (100%)	3	3 (100%)	3 (100%)
2012				45	43 (96%)	43 (96%)	17	17 (100%)	11 (65%)
2013				5	5 (100%)	5 (100%)	15	15 (100%)	15 (100%)
2014				21	21 (100%)	19 (90%)	15	15 (100%)	15 (100%)
Total	1025	573 (56%)	457 (45%)	150	142 (95%)	142 (95%)	74	72 (97%)	67 (91%)

Green sturgeon were not strongly deterred by the anomalies associated with the bridges. They migrate through the San Francisco Estuary to the upper reaches of the Sacramento River where they spawn and return through the estuary to the ocean after spawning concluded. A total of 74 inbound migration trips and 150 outbound migration trips by adult green sturgeon were monitored from 2007 to 2014 (Table 3-2). Inbound migrations were first detected at Golden Gate Bridge, then Richmond Bridge, then Benicia Bridge while outbound migrations moved from Benicia Bridge, to Richmond Bridge, to Golden Gate Bridge. Of these 74 inbound movements, 72 (97%) resulted in detections at Richmond Bridge and 67 (91%) produced detections at Benicia Bridge at the confluence of San Francisco Bay with the Sacramento-San Joaquin River Delta. Furthermore, 142 (95%) of the 150 total outbound migrations resulted in detections at the Richmond Bridge and Golden Gate Bridge. Hence, almost all of the green sturgeon entering or exiting the bay experienced the strong anomalies associated with the bridges but were not deterred from their upriver or downriver migration movements.

Discussion

Magnetic field anomalies were detected due to the presence of both the high voltage direct current Trans Bay Cable (when carrying load current) and the bridges which span the bay within the San Francisco Estuary. We found that the distortions in the earth's main field produced by bridges were much greater in intensity and distance from source than those from the Trans Bay Cable. The former anomalies exceeded the latter by over an order of magnitude. Although the cable anomalies increased strongly with depth, the bridge anomalies were not consistently stronger at either the surface or deep tows. A salmon smolt swimming along the cable would be experiencing a small anomaly, and it might utilize this to move out of the bay. However, it would encounter a much stronger anomaly as it passed underneath the bridge. Would it ignore this increase in magnetic intensity and continue on its migration out of the bay, or would it deflect its movement east or west along the bridge?

Despite the magnitude of the anomalies produced by bridges, significant numbers of tagged Chinook salmon smolts migrated downstream past the Richmond Bridge, which produced a strong magnetic anomaly, to the Golden Gate Bridge, where they were detected by dual arrays of tag-detecting monitors moored in lines across the mouth of the bay. Furthermore, over 90% of adult green sturgeon that entered the mouth of the bay during inbound migrations passed Richmond Bridge and were detected at Benicia Bridge on their way upstream to spawn in the headwaters of the Sacramento River. Outbound migrations experienced similar success, with 95% of green sturgeon traveling downstream through the San Francisco Bay being detected at Richmond Bridge and Golden Gate Bridge on their way to the Pacific Ocean. Hence, salmonids and green sturgeon are not strongly deterred by these strong magnetic anomalies that run perpendicular to their migratory route.

Substantial percentages of Chinook salmon smolts migrating downstream as well as adult green sturgeon moving upstream and downstream passed the Richmond Bridge with its strong magnetic anomaly. These are species, for which evidence exists that they use the natural ambient magnetic (or electric) fields to guide their movements [8-11], or have electroreceptors capable of perceiving magnetic fields[20]. Westerberg and Begout Anras [23] tracked 25 silver eels in the vicinity of a high voltage, direct current cable with a similar load to the Trans Bay

Cable, off the southern coast of Sweden. Approximately 60% of the eels passed over the cable during the short tracks, indicating that the cable's electromagnetic field did not obstruct their migration in a large way.[23] Coded acoustic beacons and stationary receivers, similar to those used in this study, were used to examine the effect of the electromagnetic field from a cable transmitting alternating current on silver eels in the Baltic Sea. The rates of movement of eels passing between arrays of monitors north and south of the cable were compared to rates of movement across the cable between arrays on either side. [24] The swimming speeds of 60 eels were significantly lower around the cable than both north and south of the cable. However, the behavior of the eels could not be monitored during passage, leading the researchers to conclude that further work is needed to understand the nature of the effect.

Yet some salmon smolts that were detected at the Richmond Bridge did not reach the Golden Gate. We do not know the fate of the smolts that did not reach Richmond Bridge after passing under Benicia Bridge as well as the fate of the smolts that did not pass from the former to the Golden Gate Bridge. There could be various reasons for this such as: 1) loss of life due to predation, 2) tag shedding, 3) low detection probability, or 4) mis-directed orientation. There is evidence to be presented elsewhere (Wyman et al., in prep.) that more smolts may be detected at Bay Bridge after the cable was activated than before, perhaps indicating that the cable may impact the migration movements of some fish. Westerberg and Lagenfeldt argued that an intensive tracking study is necessary to identify any effect on a migratory species.[24] We recommend that future tracking studies employ transmitters carrying a strain gauge and 3-axis accelerometer to characterize the swimming behavior of the fish as they pass over the cable and a 3-axis gradiometer to measure the strength of the EMF induced by current flowing through the cable. Two migratory species, the green sturgeon and cow shark (*Notorhynchus cepedianus*), have been tracked in the vicinity of the Trans Bay Cable and would make ideal candidates for such a study. [25, 26]

4 BEHAVIORAL RESPONSES BY MIGRATORY CHINOOK SALMON AND GREEN STURGEON TO A HIGH-VOLTAGE POWER CABLE

Introduction

Globally, there are significant existing or planned developments to secure marine-based energy sources (e.g. offshore wind farms, wave- or tidal-based power) and distribute electricity through extensive subsea cable networks. There is growing concern worldwide that the electromagnetic fields (EMFs) induced by current passing through these cables may interact and even alter the behavior and physiology of marine species (many of conservation importance), with potentially lasting effects on migration, feeding habits, reproductive potential, and population or community status[27]. However, knowledge and understanding on this topic is extremely poor [28]. Electromagnetic fields (EMF) generated by the cables that carry electric power from hydrokinetic energy generating sources to shore-based power stations will produce local distortions in the earth's main field. Concern exists that animals that migrate along the continental shelves might orient to the EMF from the cables, and move either inshore or offshore, away from their normal paths. Similar occurrences have been observed in marine species in response to naturally occurring magnetic topography: whales have been shown to strand where magnetic lineations intersect with the coastlines of Great Britain [17] and eastern coastline of North America [18] due the tectonic rotation of the oceanic plates.

The high voltage, direct current (HVDC) Trans Bay Cable (TBD) runs 85 km from the city of Pittsburg at the edge of the Delta, a network of sloughs and channels, along the south side of the main channels of Suisun and San Pablo Bays, crosses the deep flat bottom of San Francisco Bay and comes ashore at the city of San Francisco south of the mouth of the estuary. This cable was activated in 2010 and transmits approximately 400 megawatts of power at a DC voltage of +200 kV, to provide a significant portion of San Francisco's power needs. Importantly, this undersea cable run both parallel and perpendicular to the migration route of several key species of fish

within the San Francisco Bay Estuary which were already the subject of several migratory behavioral studies before the cable was activated. By comparing movement patterns and migration success before verses after the cable was activated, we can investigate how species respond to this type of environmental perturbation. Thus, the presence of the TBC and the timing of its energization produced conditions amenable to conducting a "natural" experiment as to its potential impacts on marine life in the estuary.

In this study, we examined the effect of cable activation on two anadromous fish species, late-fall run Chinook salmon (*Oncorhynchus tshawytscha*) and green sturgeon (*Acipenser medirostris)*. At the time of cable activation, the migration patterns of both species were already being examined using acoustic biotelemetry within the San Francisco Bay Watershed [3, 5-7, 19]. Late-fall run Chinook salmon smolts migrate downstream from the upper Sacramento River in the winter and early spring through the San Francisco Estuary to the Pacific Ocean where they grow into adulthood before returning to the upper river to spawn[5-7]. Similarly, green sturgeon migrate out through the San Francisco Bay to the Pacific Ocean as juveniles before returning periodically as adults to migrate upstream to their spawning grounds in the upper Sacramento River [3, 19, 25]. Previous studies have demonstrated that some salmonid species use the natural ambient magnetic or electric fields as navigational aids during migration or foraging activities [8-11]. Anatomical studies have suggested that sturgeon species may also be capable of detecting magnetic or electric fields [20].

Previously, we described the effect of the TBC's load current on the local magnetic field [21] and anomalies in the local field from bridges on traversing the migratory routes of fishes within the San Fransico Bay [29]. In this paper, we examine the potential effect of the cable's presence on the outbound migration of late-fall Chinook salmon smolts and both the inbound and outbound migrations of adult green sturgeon through the San Francisco Estuary. This involved comparing the distribution of detections of fish implanted with acoustic transmitters with coded identities at four cross-bay arrays of tag-detecting autonomous receivers to multiple variables associated with the TBC,local environment, and fish characteristics. We primarily use mixed-effects models to determine which factors influence transit times and rates, as well as movement patterns along the route, such as the first location of the fish at each array, misdirection from the

route or successful migrations. Overall, the goal of this study was to investigate whether fish movement behaviors are impacted by activation of the undersea cable and whether its activation either hinders or facilitates outward and inward migration of these two species.

Methods

Fish Data

In the early spring, juvenile late-fall run Chinook (LFC) salmon migrate from their spawning grounds in the upper rivers through the San Francisco Bay to the Pacific [5, 6]. Adult green sturgeon (GS) enter the San Francisco Bay in winter and spring and migrate upstream to spawning sites in the upper Sacramento River and its tributaries [3, 19] before migrating back downstream through the San Francisco Bay to the ocean after spawning is complete. This study utilizes fish movement behavior data from previous biotelemetry studies carried out on LFC salmon smolts and green sturgeon both before and after the Trans Bay Cable was installed through the San Francisco Bay. These detections provide an ideal natural experiment to examine the impact of the TBC activation on fish migration. In these studies, fish were tagged with uniquely coded ultrasonic transmitters (VEMCO, Inc. V7 through V16) and detected throughout the San Francisco Bay by receivers attached to bridges or anchored on the channel bottom. Along with the historical fish detection data from the Biotelemetry Laboratory at the University of California-Davis, we obtained permission to use additional detection of the two species from the following agencies and organizations: National Oceanic and Atmospheric Administration (NOAA), National Marine Fisheries Service, US Bureau of Reclamation, California Department of Water Resources, California Department of Fish and Wildlife, Oregon Department of Fish and Wildlife, Washington Department of Fish and Wildlife, US Fish and Wildlife, East Bay Municipal Utility District, US Army Corps of Engineers, and H.T. Harvey and Associates.

Data available for each tagged fish included detection dates and locations, fish length and weight at tagging (weight for LFC only, incomplete lengths for sturgeon), tagging date, and release location. For LFC, detection year was subsequently coded as the year in which the bulk of detections for each release cohort occurred, and as such, fish that were detected in the Bay in late December were included in the subsequent detection year with the majority of their release cohort. The body condition factor (K) of each LFC smolt was calculated for this study using the

fork length and weight measurements collected during tagging activities. These data were incorporated into the following equation developed by Fulton [30]:

$$K = (10^5 \times W)/L^3$$

where W is mass (measured in grams) and L is fork length (measured in mm). Release locations, defined as the location where fish were released post-tagging, were categorized into three regions per species for this study. For LFC, release locations were generalized as occurring either in the upper Sacramento River (upstream from Colusa), the middle Sacramento River (from Colusa to Sacramento), or the Sacramento-San Joaquin Delta (downstream of Sacramento). For sturgeon, release locations were defined as occurring either in the Sacramento River (from Sacramento to all locations upstream), the Sacramento-San Joaquin Delta (all location between Sacramento and the Golden Gate Bridge), or Oregon and Washington (all locations within these two states). Length of sturgeon was not included in any fitted models in this study because these data were not available for all fish. Removing fish without lengths would result in a loss of 7.9% (6 of 76) of inbound sturgeon and 9.6% (16 of 167) of outbound sturgeon. Importantly, the removal of these fish would be biased towards fish present when the cable was active rather than inactive: 100% of the inbound fish without lengths and 75% of the outbound fish without lengths were detected when the cable was active (representing 12.2% of all inbound fish and 16.9% of all outbound fish during cable active periods). Therefore, to prevent a disproportionate removal of adult fish during these important time periods based on lengths alone, we did not include length or any estimate of length in the model selection. However, we do acknowledge that length likely effects fish movement behaviors within the Bay.

Magnetometer Survey

Magnetic field surveys were conducted at four locations in the San Francisco Bay between July 10th and August 8th, 2014. The surveyed areas overlapped with acoustic telemetry arrays situated along the Benicia-Martinez Bridge, the Richmond-San Mateo Bridge, and the Oakland-Bay Bridge, along with a non-bridge location in San Pablo Bay (Figure 2-1). Surveys were performed with a gradiometer comprised of twin cesium magnetometers separated from each other by 1.5m (G-882 TVG , Geometrics, Inc., San Jose, CA) towed from a research vessel. Survey lines were orientated 1) perpendicular to the TBC (and parallel to the fish detecting

arrays), and 2) perpendicular to the bridges. See Kavet et al. (2016) and Klimley et al. (in prep) for details on the design and execution of this survey.

The measurements of magnetic field intensity were post-processed and mapped using MagPick magnetometer data processing software (Mikhail Tchernychev, http://sourceforge.net/projects/magpick/). Post-processing included the following: 1) differentially correcting the GPS points to get sub-meter accuracy on survey locations using GPS software (Trimble GPS Pathfinder Office, Trimble Navigation Ltd.), 2) correcting for tidal stage based on tidal stage data downloaded from the nearest port stations operated by the National Oceanic and Atmospheric Administration, NOAA, 3) correcting for diurnal and other variations in the Earth's magnetic field by subtracting the magnetic field measures recorded at the Jasper Ridge Biological Preserve base station from field measures, and 4) removing DC offset between the two magnetometers. The stages 2) and 3) were carried out using the MagPick universal regex parser plugin.

After post-processing was complete, two types of maps were interpolated for each area using the survey lines that run parallel to the bridges/arrays. The first is a map of total magnetic field intensities that illustrates the anomalies present in the area, calculated as the magnetic fields measured by the magnetometers minus the Earth's magnetic field variation. The second is a gradient map (or quasi-analytic signal map), which depicts the rate of change in anamolies in the magnetic field (in nT/m), calculated using 1) the transverse component of the gradient vector of the total magnetic field using the difference of the two magnetometers divided by their 1.5 m separation, 2) the longitudinal component of the gradient vector utilizing the average of the two magnetometers and the data collected along the survey line, and 3) the estimated vertical derivative of the gradient vector (see Tchernychev 2013 for details [22]).

The resulting maps of the total magnetic field and gradient illustrated the magnetic signature produced by the TBC, depicted as a linearly-orientated series of positive and negative spikes traveling perpendicular to the bridges and arrays of acoustic monitors (Figure 3-2). The intensity of the magnetic anomaly produced by the TBC was measured using profile plots of the measured magnetic field minus the Earth's magnetic field on the y axis and the distance along the survey track on the x axis. The measurement data were entered into a regression model based on

fundamental magnetostatics to derive estimates of the cable load current, its buried depth and angle of twist relative to the horizontal [21] The height of the magnetometer above the water's bottom, the angle of the survey line relative to east-west, and the values of the mutually orthogonal background geomagnetic field vectors form online sources were empirical inputs. The modeling reported a strong correlation (Pearson r>0.99) between modeled and measured anomalies, a cable burial dept of nominally ~2m (consistent with unpublished 6-foot value), and load currents consistent with the cable's 1,000 A rating. Subsequently, Klimley et al. (in revision) described the large magnetic anomalies caused by the bridges.

Environmental Data

Environmental conditions found along the path of fish migration through the San Francisco Bay may vary both spatially and temporally. In order to assess the influence of these factors on the migratory behavior of the two fish species, we quantified environmental propertiesnear the time and location of fish detection events. These data included measurements of TBC cable load, distance to the cable, channel depth, total magnetic field intensity and gradient, time of day (as day/night), tidal current strength and direction, temperature, and discharge.

Installment of the TBC in San Francisco Bay began in 2009, with the cable officially activated on November 23, 2010. The average daily load data (MW) carried by the TBC from this date forward was provided by Trans Bay Cable LLC. However, since we did not know when the cable was being tested prior to official activation, we conservatively decided not to include any fish detections from January 1, 2010 to November 23 2010 in our fish behavior analysis.
The distance to cable, channel depth, and magnetic field measures were quantified in ArcMap at all receiver locations in the arrays at Benicia Bridge, Richmond Bridge, and Bay Bridge, as well as the bridge-free array in San Pablo Bay. Depth and magnetic field intensities were calculated in both at the point locations of the array receivers and averaged across the detection range of the receivers for the different types of acoustic transmitters Tests were carried out to estimate the range over which the coded acoustic pulses emitted by the transmitters were detected by the hydrophone receivers within the study locations. Range tests were conducted using three 69 kHz VEMCO brand transmitter types (tags): V7-4L (136 dB re: 1 µP @ 1 m), V9-2L (146 dB), and V16-6L (152 dB), similar in size and power to the range of transmitters used in the detection data for this study. Testing occurred at Richmond Bridge because it was a geographical midpoint

between all the locations used in this study. Tags were submerged near the center of the bridge and left to operate for one month. During this time, each tag emitted a unique ping at a fixed interval of 15 minutes. After one month, all the receivers attached to Richmond Bridge were downloaded and their detection records were used to calculate the average detection range of each transmitter. This was accomplished by calculating the detection efficiency of each tag at each receiver (dividing the average number of received detections by the actual number of transmitted pulses), graphing efficiency versus distance from tag for each receiver, and using the best fit trend line of this plot to calculate the distance at which the transmissions from each tag could be detected with an average efficiency of 75%. This distance was 70 m for the V7 tag (representing all LFC smolt tags), 225 m for the V9 tag, and 275 m for the V16 tag (representing all adult green sturgeon tags). Although these values will vary at different locations, environmental conditions, and receiver positions in the San Francisco Bay, this month long range detection test provided a robust estimate of detection range that was used to more accurately average the environmental data surrounding each receiver.

Depths were determined from a digital elevation model (DEM) of the San Francisco Bay constructed by the National Oceanic and Atmospheric Administration (NOAA) (http://www.ngdc.noaa.gov/dem/squareCellGrid/download/741). The DEM has a 1/3 arc-second (~10 meter) cell size, and is referenced to a vertical datum of NAVD 88 which uses Mean High Water as its tidal reference (Carignan et al 2011). The point data from the total magnetic field and quasi-analytic signal maps were exported from MagPick and imported by ArcMap, then re-interpolated using the inverse distance weighting method to create geo-referenced raster images of the measured magnetic fields. The magnetic field measurements include total field (expressed in nT, minus Earth's magnetic field) and quasi-analytic signal which measures the rate of change in nT/m.

Tidal current velocity and direction data were obtained from weather stations operated by NOAA within the San Francisco Bay at locations between 0.2 and 0.82 nautical miles from our detection arrays. Data were accessed from the Current Prediction section of the NOAA Tides and Currents webpage (http://tidesandcurrents.noaa.gov/noaacurrents/Stations?g=696) , whichincludes the time of maximum current and slack current, as well as the magnitude and direction of maximum

current. We assigned a binary level tidal current strength (i.e., strong/weak) and direction (i.e., in/out) to each fish detection for the tidal currents recorded at the nearest station and the time of the detection. Each detection was also assigned a binary day/night variable based on the time of detection. For Chinook smolts the cut off between day and night was based on the average sunrise and sunset times for the few months in which they traveled through the San Francisco Bay (sunrise: 700, sunset: 1730 hrsPST). However, since green sturgeon travel through the San Francisco Bay throughout the year during their inbound and outbound migrations instead of during a narrow seasonal period like the Chinook smolts, we assigned day and night classifications based on the date of the detection, the GPS location of the detecting receiver, and day and location specific sunrise and sunset times as calculated by the sunriset function in the R package maptools [31]

Water temperature (°F, sampled hourly) and discharge (f^3/s, sampled daily) measurements were utilized from the Port of Chicago and Delta Outflow environmental stations, respectively, positioned at the transition between the Sacramento-San Joaquin Delta and the San Francisco Bay. These recordes were accessed through the California Data Exchange Center (www. http://cdec.water.ca.gov/)..

Fish Detections

Detections from 763 late-fall Chinook salmon smolts were available from 2007 through 2011. Data quality filters were applied to remove spurious detections, incorrect identity tags, and fish that were in older age classes than Chinook smolts (fork length < 315 mm).

Detections from 368 green sturgeon were collated in preparation for this analysis. A variety of filters were applied to the sturgeon data set in order to promote data quality and to correctly classify the migration types. Only reproductively mature adult green sturgeon were included in this analysis, defined as fish with a fork length of at least 1390 mm [32]. Since, no fish with recorded fork lengths below the threshold of 1390 mm were detected in the spawning grounds of the upper Sacramento River (>400 rkm), sturgeon without recorded lengths were also counted as adults if they were detected in the Sacramento River above 400 rkm and were tagged with the larger V16 tags. Classification of sturgeon movements as inbound migrations required the fish to enter into San Francisco Bay between January and June and to be detected above 100 river km

(rkm, with 0 rkm occurring at Golden Gate Bridge) within the Sacramento River Watershed in the direction of their spawning grounds. Outbound sturgeon migrations were defined by the detection of fish above 100 rkm before being detected in the Bay. As a reference to river km, the Richmond Bridge array is located at 14.7 rkm, the Carquinez Bridge array at 41.5 rkm, and the Benicia Bridge array at 51.7 rkm. To ensure that the migration movements were not influenced by any capture and handling effects [33], we did not include any migration movements that began less than 30 days after tagging. Detections were also removed if individuals were only seen at one location upstream of the Bay and if there were in general fewer than 5 detections in the system (from Sacramento River through the San Francisco Bay).

Fish Behavioral Variables

Binary descriptors of migration

Binary migration descriptors (yes or no data) were assigned to each fish's migration movements based on whether or not they present on both sides of the cable location, at the Golden Gate or at theBay Bridge. The variable *Cable Cross* indicated if fish were detected on both sides of the cable location at some point during their migration (i.e., to the left and to the right of the cable location, either before or after the cable was installed, as labeled from the out-migration point of view for consistency). For this designation, we examined fish detections on all receivers operated in the bay (~245), not just the 113 receivers at the specific array locations of Benicia Bridge, Carquinez Bridge, San Pablo Bay, Richmond Bridge, and Bay Bridge. When a fish was detected at a Bay Bridge receiver, we defined that migration movement as being *Misdirected*, since the Bay Bridge is south of the migration path in and out of the bay. When an outbound migrating fish was detected at a Golden Gate receiver or when an inbound fish was detected at a Carquinez or Benicia receiver, we assigned that migration as having a *Successful Exit*.

Survival analysis

In addition ot calculating the percentage of successful exits through the San Francisco Bay for each yearly cohort of Chinook salmon, we also conducted a survival estimate of Chinook which estimates both “survival” through the San Francisco Bay and the detection probabilities of the arrays. Survival may be influenced by factors such as alternate movement paths, tag shedding, predation, or non-predation deaths. Detection probabilities are important to account for as the probability of detecting fish at the arrays may change due to mechanical, environmental, or

behavioral processes. For example, the water discharge rates in the bay periods of Chinook salmon migration is different across years, which can potentially impact the detection probabilities of the receivers in the arrays (i.e., high discharge could result in lower detection efficiency) and thus impact the resulting survival probabilities estimated using the fish detections. Therefore, we estimated the survival probabilities of fish reaching the Golden Gate from Benicia Bridge using techniques from mark-recapture models [34]. Mark-recapture models are a powerful tool to estimate survival because they simultaneously estimate both detection and survival probabilities. Survival probabilities for green sturgeon were not calculated as this type of analysis is not as applicable to this species. The adult sturgeon monitored do not experience large scale mortality during their migrations after they reach adulthood.

The Cormack-Jolly-Seber (CJS) mark-recapture model estimates two parameters: 1) S_i: the probability of surviving between receiver array i to i +1, and 2) p_i: the detection probability at array i conditional on the fish surviving to arrive at array i. Figure 4-1 illustrates how the CJS model would be applied to the conditions in our study system. The CJS model is based on a multinomial probability distribution representing the probability of occurrence of events in particular categories [34]. In this case, the categories are the possible detection histories of individual fish. As we are interested in examining the behavioral movements and migration success of the fish after they enter the bay at Benicia Bridge, the array at this location effectively becomes our "release site" for the fish (e.g., out of all the fish detected at Benicia Bridge, how many successfully navigate to the mouth of the Pacific Ocean at Golden Gate Bridge?). The location at Golden Gate Bridge is covered by two parallel arrays a short distance apart. These parallel arrays were put in place to increase the probability of detection at Golden Gate as fish exited the bay (i.e., if fish were missed at the eastern most array, there is a chance they could be picked up by the western most array). In the context of the CJS survival parameters, S_1 is the probability of fish surviving between Benicia Bridge and the Golden Gate East (GGE) array, while S_2 is the probability of fish surviving between the GGE array and the Golden Gate West (GGW) array. In the context of the CJS detection parameters, p_2 estimates the probability of detection at GGE, while p_3 estimates the probability of detection at GGW. Benicia Bridge, as the "release site", is p_1 and is set to 1. The goal of our investigation with this configuration of arrays was to estimate S_1 (survival probability between Benicia and GGE).

Figure 4-1 Representation of the Cormack-Jolly-Seber model for calculating survival probability estimates adapted to the study location.

A schematic of the CJS model applied to this study system is depicted on the left with the maximum likelihood estimator equations and sample data for this model illustrated on the right.

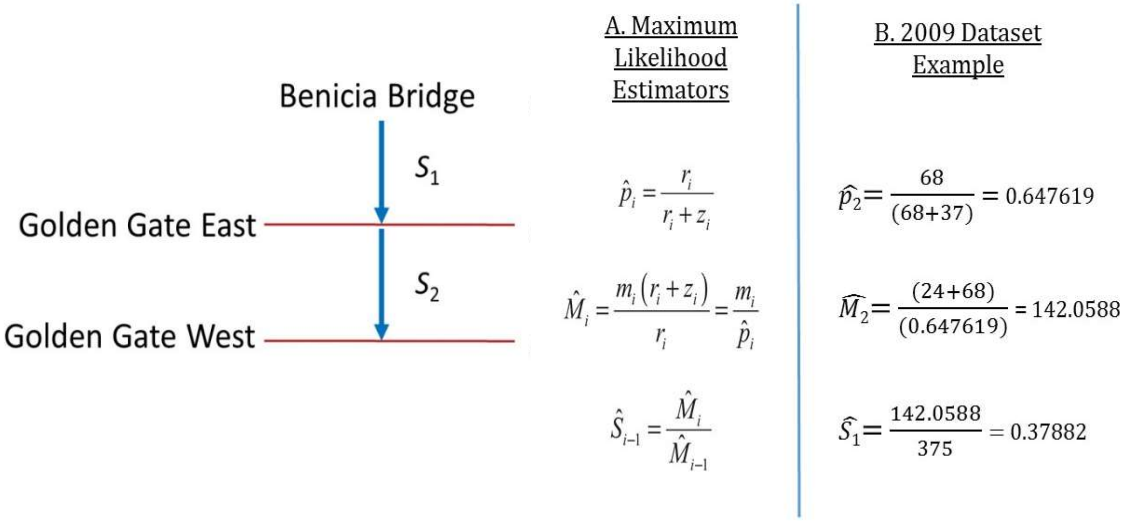

Transit time and rate

Transit rate or time was calculated per fish per reach as the total amount of time in hours between the last detection of a particular fish at an array on one edge of a reach and the first detection of that fish at the subsequent array at the opposite end of that reach. The numbering of reaches corresponds to the order of reaches the fish travels through during their migration (e.g., an inbound sturgeon will travel through GS_In_1 first). Transit timesfor LFC smolts for for outbound migrations were calculated with three reaches: *Reach 1* between the arrays at Benicia and Richmond Bridges, *Reach 2* between Richmond and Golden Gate Bridges, and *Reach 3* as the total distance between Benicia and Golden Gate Bridges. Transit times of outbound adult green sturgeon were calculated within three similar reaches including *Reach 1* between the arrays at Carquinez and Richmond Bridges, *Reach 2* between Richmond and Golden Gate Bridges, and *Reach 3* as the total distance between Carquinez and Golden Gate Bridges. Transit times of inbound adult green sturgeon were calculated within three reaches, including *Reach 1* between Golden Gate and Richmond Bridges, *Reach 2* between Richmond and Carquinez Bridges, and *Reach 3* as the total distance between Golden Gate to Carquinez Bridges. Chinook

smolts typically show very directed outbound movements through the Bay with most individuals traveling between Benicia Bridge and Golden Gate Bridge in less than a week [5] Conversely, adult green sturgeon exhibit more variability in direction of movement, stoppages, and rates of movement. Carquinez was used as a reach border for sturgeon instead of Benicia because the array at Carquinez was installed earlier than the array at Benicia, thus allowing more data to be utilized on green sturgeon movements within the bay.

If an outbound Chinook smolt was detected at a downstream array and then subsequently detected back at an upstream array (e.g., detected at Richmond Bridge, then at Benicia Bridge), that fish was removed from the analysis. Since we could not determine if large scale 'backwards' movements were due to tidal influences, predation (i.e., the smolt was predated and the tag is traveling within the predator before excretion), or directed movements, removing these fish from the analysis was determined to be the most conservative approach. In contrast, some green sturgeon may travel back and forth between arrays before ultimately continuing on their upstream or downstream migration. For these fish, we only included the first transit time across each reach in our analysis instead of including subsequent movements across the same reach to standardize measures between all fish.

Location of first presence

Lastly, we examined influences on migration movements by assessing what factors predicted the location of LFC at their first detection at several arrays. This was defined as the location of the first acoustic receiver where a fish was detected at as they migrated through the bay (referred to as 'first presence' location). This 'first presence' analysis provides a snap shot of where a fish was traveling before it encountered any potential interference from the cross-channel bridge structures that several of the arrays stretched across. Acoustic arrays used for this analysis included those situated at Benicia and Richmond bridges along with a non-bridge array in San Pablo Bay.

Statistical Analysis

A combination of logistic and linear mixed-models were used to investigate migration movements of fish in relation to environmental, behavioral, and individual variables. Mixed models allowed us to account for occasional repeated measures within sturgeon (e.g., some

sturgeon were tracked during multiple years) and to assign random effects to the models to account for additional variation.

Logistic regression mixed effects models were developed to assess which factors influence the probability of fish 1) crossing the location of the cable during their migration route, 2) being misdirected to Bay Bridge during their migration, and 3) successfully traveling through the Estuary. Binary response variables included *Cable Cross*, *Misdirection*, and *Successful Exit*. Possible fixed effects entered into these models included three environmental variables (cable activity as a binary on/off variable, river discharge, and temperature), two individual variables (K factor for LFC, and release location for both species), and two behavioral variables (binary variables indicating misdirection and cable location crossing, where appropriate). A single river discharge and temperature measure was used for each fish migration, representing the conditions observed at the Port of Chicago and Delta Outflow environmental stations during the first detection of that fish in the Bay. Release location was included as a fixed effect because Michel et al. (2013) indicated it can influence LFC smolt transit rates through the Sacramento River Watershed. Random intercepts included fish identity and detection year. Fish identity was included as a random effect in the sturgeon models because some fish were detected during multiple migrations (e.g., repeated measures for some fish). Year was included as a random effect for both species as environmental conditions may vary generally between years (e.g., wet vs. dry years).

We examined what factors influenced transit time (hr) of outbound and inbound migrations using linear mixed models with maximum likelihood estimates of parameters. Separate models were developed for each of the three reach locations with transit time as the response variable. Fixed and random effects entered into these models were the same as for the logistic regressions listed above. To determine if outliers played a large role in transit time model outcomes, model selection procedures were re-run after removing extreme outliers from the dataset. Extreme outliers were defined as transit times with values beyond three times the interquartile range. Details of the full model selection based on these trimmed datasets are not provided here, but for each transit time analyses, we contrast the best model results obtained with the full dataset with that of the trimmed dataset. However, a strong biological reason needs to be provided to use the

trimmed data in place of the full dataset. For example, since the majority of Chinook smolts rapidly transit through the bay in a directed fashion, any unusually long transit times may represent spurious detections (e.g., from predated individuals). In contrast, longer transit times by some individual green sturgeon may represent biologically relevant and valuable data points in relation to responses to environmental conditions.

Additional analyses were conducted to test whether transit times (for GS) and transit rates (for LFC) were significantly different 1) when the cable was active versus not active, 2) during migrations where the fish were seen on both sides of the cable location versus migrations where they were not and 3) during migrations where fish were detected at Bay Bridge versus migrations where they were not. Examinations of transit time (hr) and rate (km/hr) were conducted using Welch t-tests if parametric assumptions were met (means reported), and nonparametric Mann Whitney U tests if they were not (medians reported).

Logistic regression models were also developed to determine what factors predicted the location where fish were first detected at three arrays. The binomial response variable was the first presence location of fish at each array (i.e., the first receiver per array that a fish was detected at was scored with a 1, while all other receivers in that array scored a 0). The environmental predictor variables entered into the model included channel depth (m), total local magnetic field (nT) and the rate of change in total local magnetic field (nT/m) at the surface and at depth, distance to cable (m), cable load (average MW/day), day/night, tidal current strength, tidal current direction, temperature, and river discharge. Individual variables included K factor for LFC and release location for both species. Random effects were fish identity and receiver identity nested within array location, both with random intercepts. The distance between the receiver and the cable location was the same before versus after the cable was activated: the distance of detections at periods before activation refers to the eventual location of the cable. As a note, all depth and magnetic field data were derived from the point locations of the receivers and not the average value of these variables over the detection range of the receivers because of strong correlations between these values.

For all mixed-effect models, the most appropriate candidate models were selected by comparing fuller models against reduced models or null models using AIC comparison and likelihood ratio tests through ChiSquare statistics in the anova function. If there was no significant difference found between models, the parsimony principal dictates that we choose the most reduced model. The significance of fixed effects within the mixed models were determined using t-tests with Satterthwaite approximations to degrees of freedom [35] .

All analyses used two-sided tests using 0.05 significance levels. Model assumptions of linearity, homoscedasticity, and normality were assessed using QQ plots, residuals versus fitted values plots, spread level plots, and box plots of the residuals versus independent variables. Statistical tests were performed in R 3.3.1 [36] using primarily the following packages ggplot2 [37], lme4 [38], lmerTest [35] and AICcmodavg [35] .

Results

Detections from 763 outbound migrating late-fall Chinook salmon smolts from 2007, 2008, 2009, and 2011 were analyzed in this study (Table 4-1). Chinook smolts used in this analysis had an average fork length of 165.24 mm ± 15.16, average weight of 52.48 g ± 17.00, and average K factor of 1.12 ± 0.09. A total of 167 outbound migrations from 142 adult green sturgeon and 76 inbound migrations from 74 adult green sturgeon were analyzed in this study. Detections from outbound movements occurred yearly between 2006 and 2014 while inbound detections occurred yearly between 2007 and 2015. Out of a total of 154 unique fish, 15 were female, 40 were male, and 99 were of unknown gender. The average fork length measured during capture and tagging ranged from 1440 to 2400 mm (mean ± SD: 1734.11 mm ± 154.14).

Table 4-1 Summary of Chinook salmon fish detection data.

The column "Exit" shows the original calculation of the percentage of fish detected at Benicia that were also detected at Golden Gate (i.e., successful exit). The column "Survival Probability" shows the estimated proportion of fish who successfully exited the bay using mark-recapture models. The year 2010 is not listed as we do not know if the cable was operational at that time.

Year	Total Fish (#)	Cross Cable (#,%)	MisDirect (#,%)	Exit (#,%)	Survival Probability
2007	40	28 (70%)	1 (3%)	25 (63%)	65.6%
2008	148	112 (76%)	9 (6%)	61 (41%)	42.5%
2009	424	276 (65%)	67 (16%)	151 (36%)	37.9%
2011	151	138 (91%)	42 (28%)	57 (38%)	37.5%

Crossing Cable Location

The percentage of Chinook smolts that were detected on both sides of the cable location during the same migration trip (indicating the fish crossed the cable location at some point during their migration) increased after the cable was activated, from an average of 70.3% before cable activation to 91.0% in 2011. However, cable activity did not significantly predict if Chinook smolts would cross the cable location (Table 4-2), although smolts were less likely to cross this location when temperatures were higher ($ß = -0.21$, $p < 0.0001$).

The proportion of outbound migrations by green sturgeon that involved crossing over the location of the cable increased from 85.1% (57 of 67) during periods of cable inactivity to 100% (71 of 71) after the cable was activated. However, neither cable activity nor any other fixed effect variable significantly predicted whether geen sturgeon crossed the cable location (Table 4-2) In contrast to the outbound migrations, every inbound migration involved crossing over the cable location, both before and after the cable was activated (18 and 67 migrations, respectively).

As such, a model predicting which fixed factors influenced the probability of crossing the cable location for inbound sturgeon was not investigated.

Table 4-2 Candidate model selection for predictors of crossing the cable.

Candidate logistic regression models are ordered by their Akaike's Information Criterion (AIC) score. The best model (in bold) for each species and migration type was determined based on AIC comparison and log likelihood tests. Information provided includes the fixed and random effects for each model as well as the number of parameters (k), the AIC score, and the log likelihood (logLik) values.

Species, Migration	Models	k	AIC	logLik
LFC Outbound	CC~T+RL+(1|Year)	5	301.52	-145.76
	CC~T+(1|Year)	3	302.31	-148.16
	CC~T+RL+C+(1|Year)	6	302.6	-145.3
	CC~T+ RL+K+C+(1|Year)	7	304.25	-145.13
	CC~1+(1|Year), Null	2	315.74	-155.87
	CC~T+RL+(1|Year)	5	301.52	-145.76
GS Outbound	**CC~1+(1|ID)+(1|Year), Null**	3	31.96	-12.98
	CC~T+(1|ID)+(1|Year)	4	33.82	-12.91
	CC~T+D+(1|ID)+(1|Year)	5	36.9	-13.45
	CC~T+D+C+(1|ID)+(1|Year)	6	37.63	-12.82
	CC~T+D+RL+C+(1|ID)+(1|Year)	8	38.93	-11.46

C = cable active (n/y), CC = cable cross (n/y), D = discharge, ID = fish identity, K= K factor, RL = release location, T = temperature

Figure 4-2 Transit rates of outbound Chinook smolts during periods of cable inactivity and activity.

Box plots of transit times are shown for the segments between Benicia Bridge and Richmond Bridge (left), Richmond Bridge to Golden Gate Bridge (middle), and Benicia Bridge to Golden Gate Bridge (right). The upper row of plots displays the full dataset and the lower row displays the trimmed data without extreme outliers.

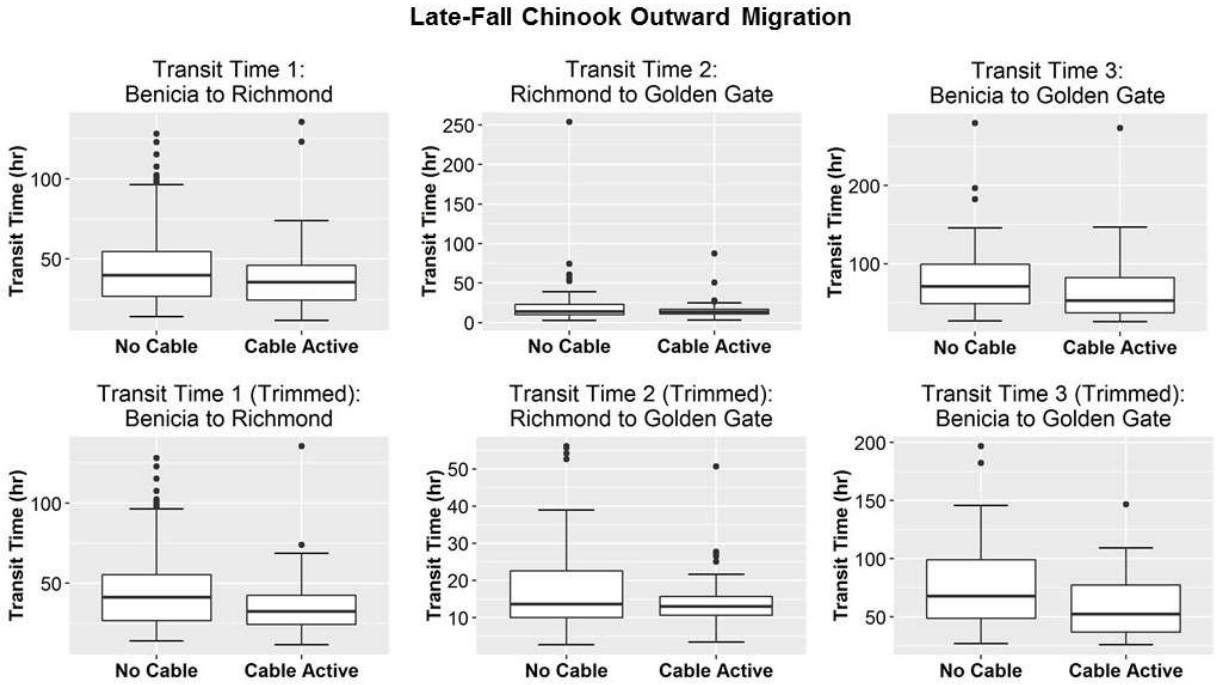

'Misdirection' to Bay Bridge

The proportion of LFC smolts that were detected at Bay Bridge increased from an average of 8.3% before activation to 28.0% after activation and cable activity predicted a significant increase in the probability of misdirection of smolts to Bay Bridge (ß = 1.21, p = 0.004, Table 4-3). Smolts with higher body condition (K factor) were also more likely to be misdirected to Bay Bridge (ß = 3.25, p = 0.011).

The array at Bay Bridge was operational during 143 (85.6%) outbound migrations and 74 (97.4%) inbound migrations of green sturgeon. Of these outbound migrations, 9.0% involved fish detected at Bay Bridge during periods of cable inactivity and 11.3% of migrations contained detections at Bay Bridge during periods of cable activity. Cable activity did not predict the probability of outbound sturgeon being detected at Bay Bridge, but increased temperature predicted a significant increase in the probability of misdirection (ß = 0.11, p = 0.017, Table 4-3). For inbound migrations occurring when the Bay Bridge array was operational, 29.4% of

migrations involved detections at Bay Bridge when the cable was inactive, while 22.9% of migrations contained Bay Bridge detections when the cable was active. No fixed effects significantly predicted misdirection of inbound green sturgeon to Bay Bridge.

Table 4-3 Candidate model selection for predictors of misdirection at Bay Bridge.

Candidate logistic regression models are ordered by their Akaike's Information Criterion (AIC) score. The best model (in bold) for each species and migration type was determined based on AIC comparison and log likelihood tests. Information provided includes the fixed and random effects for each model as well as the number of parameters (k), the AIC score, and the log likelihood (logLik) values.

Species, Migration	Models	k	AIC	logLik
LFC Outbound	MD~T+K+C+(1|Year)	5	606.16	-298.08
	MD~K+C+(1|Year)	4	607.48	-299.74
	MD~T+RL+K+C+(1|Year)	7	609.66	-297.83
	MD~T+D+RL+K+C+(1|Year)	8	611.6	-297.8
	MD~1+(1|Year), Null	2	612.89	-304.45
GS Outbound	**MD~T+(1|ID)+(1|Year)**	4	79.57	-35.79
	MD~T+ RL+(1|ID)+(1|Year)	6	81.03	-34.52
	MD~ T+D+RL+(1|ID)+(1|Year)	7	81.2	-33.6
	MD~T+D+RL+C+(1|ID)+(1|Year)	8	83.16	-33.58
	MD~1+(1|ID)+(1|Year), Null	3	84.23	-39.12
GS Inbound	**MD~1+(1|ID)+(1|Year), Null**	3	79.65	-36.82
	MD~C+(1|ID)+(1|Year)	4	81.45	-36.72
	MD~D+C+(1|ID)+(1|Year)	5	83.34	-36.67
	MD~T+D+ C+(1|ID)+(1|Year)	6	85.34	-36.67
	MD~T+D+RL+C+(1|ID)+(1|Year)	8	86.85	-35.42

C = cable active (n/y), D = discharge, ID = fish identity, K= K factor, MD = misdirect (n/y), RL = release location, T = temperature

Successful migration exits

Survival estimates indicate that the highest proportion of LFC smolts exited the San Francisco Bay in 2007 (65.5%), with survival dropping to 42.5%, 37.9%, and 37.5% in 2008, 2009, and 2011, respectively (Table 4-1). Survival estimate results are very similar to the more simplistic method of calculating the proportion of fish from Benicia that are then later seen at Golden Gate (Table 4-1). Cable activity did not predict whether LFC smolts successfully exited the San Francisco Bay Estuary, although probability of detection at Bay Bridge, temperature, and release location were included in the best fit model of exits (Table 4-4). Fish were more likely to successfully exit the system when they were detected at Bay Bridge ($ß = 1.63$, $p < 0.001$), when temperatures were lower ($ß = -0.08$, $p = 0.01$), and when they were released from the Sacramento-San Joaquin Delta as opposed to the middle section ($ß = -0.63$, $p = 0.018$) and upper section ($ß = -0.82$, $p = 0.006$) of the Sacramento River.

The proportion of outbound migrating green sturgeon that were detected at Golden Gate was 97.0% during periods of cable inactivity and 93.0% during periods of cable activity. The proportion of inbound migrating green sturgeon detected at Benicia Bridge (i.e., indicating successful transit through the San Francisco Bay) was 94.4% during periods of cable inactivity and 95.9% after the cable was activated.

Table 4-4 Candidate model selection for predictors of successfully exiting the San Francisco Bay Estuary.

Candidate logistic regression models are ordered by their Akaike's Information Criterion (AIC) score. The best model (in bold) for each species and migration type was determined based on AIC comparison and log likelihood tests. Information provided includes the fixed and random effects for each model as well as the number of parameters (k), the AIC score, and the log likelihood (logLik) values.

Species, Migration	Models	k	AIC	logLik
LFC Outbound	**EX ~T+RL+MD+(1|Year)**	6	876.63	-432.32
	EX~T+D+RL+MD+(1|Year)	7	876.63	-431.31
	EX~T+D+RL+K+MD+(1|Year)	8	878.45	-431.22
	EX~T+D+RL+K+C+MD+(1|Year)	9	880.24	-431.12
	EX~T+D+RL+K+C+MD+CC+(1|Year)	10	882.05	-431.02
	EX~1+(1|Year), Null	2	935.89	-465.94

C = cable active (n/y), CC = cable cross (n/y), EX = exit (n/y), D = discharge, ID = fish identity, K= K factor, MD = misdirect (n/y), RL = release location, T = temperature

Transit times and rates

Table 4-5 and Figure 4-2 provide a descriptive summary of LFC smolt transit times through the three reaches during periods of cable inactivity and activity, as well as periods when cable activity was unknown (1/1/2010 – 11/22/2010). Descriptive summaries of the transit times of outbound and inbound green sturgeon within the three reaches are provided in Tables 4-6 and 4-7 and Figures 4-3 and 4-4 for periods of cable inactivity, cable activity, and unknown periods.

Linear mixed effects models indicated that LFC smolts traveled faster through the first reach of their migration route when river discharge was high (ß = -0.013, $p < 0.001$, Table 4-8) and their average transit time through the second reach from Richmond to Golden Gate was significantly increased by over 10 hours if they were misdirected to Bay Bridge along the way (ß = 10.55, p <

0.004) (Table 4-8), although an examination of the data indicates this latter finding may be the result of a single large outlier. Furthermore, temperature and release location were included as fixed effects in the best fit model for smolt transit times through the whole estuary from Benicia to Golden Gate. Smolts traveled through the system more quickly in warmer water (ß = -2.32, p = 0.015) and when they were released higher in the watershed (middle Sacramento River release: ß = -16.01, p = 0.032; upper Sacramento River release: ß = -22.96, p = 0.077).

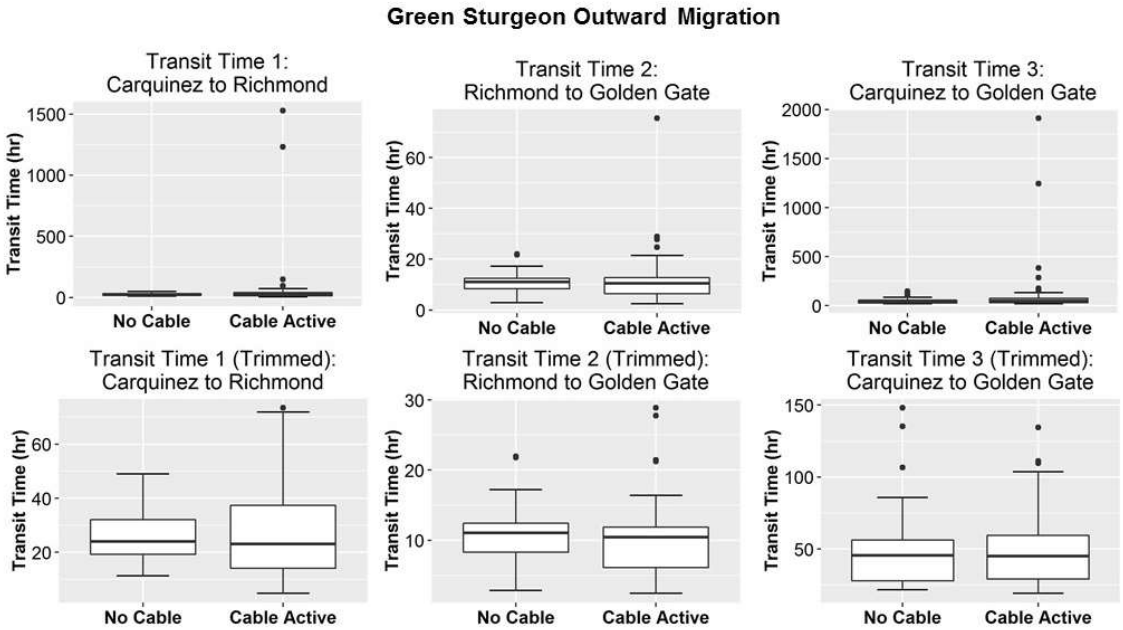

Figure 4-3 Transit times of outbound adult green sturgeon.

Box plots of transit time calculated from outbound migrations are shown for three reaches: Reach 1 = Carquinez Bridge to Richmond Bridge (left), Reach 2 = Richmond Bridge to Golden Gate (middle), and Reach 3 = Carquinez Bridge to Golden Gate (right). The upper row of plots displays the full dataset and the lower row displays the trimmed data without extreme outliers.

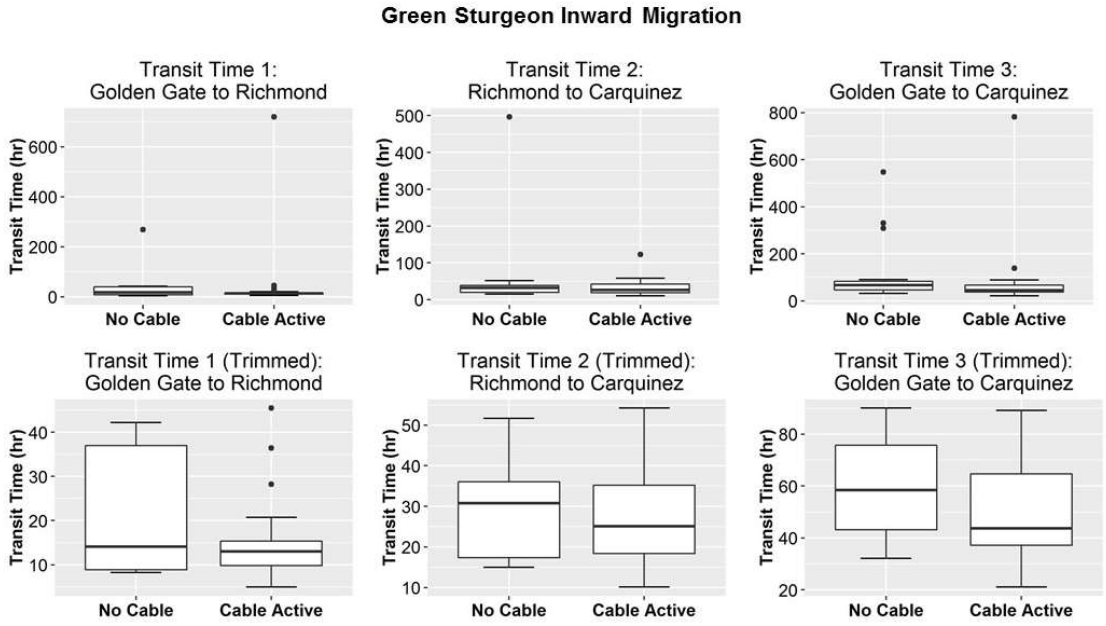

Figure 4-4 Transit times of inbound adult green sturgeon.

Box plots of transit time calculated from inbound migrations are shown for three reaches: Reach 1 = Golden Gate to Richmond Bridge (left), Reach 2 = Richmond Bridge to Carquinez Bridge (middle), and Reach 3 = Golden Gate to Carquinez Bridge (right). The upper row of plots displays the full dataset and the lower row displays the trimmed data without extreme outliers.

When extreme outliers were removed, the model selection procedures produced only slightly different results. In the trimmed dataset, transit time of LFC in the first reach was decreased by both discharge and temperature while the best fit model of transit time in the second reach only included K factor and not misdirection to Bay Bridge. This result is likely due to the removal of a large outlier associated with misdirection, revealing that better conditioned smolts tended to travel through the system more quickly (ß = -16.73, p = 0.054). Lastly, temperature and release location maintained similar influences over travel times through the whole system from Benicia to Golden Gate within the trimmed dataset.

Table 4-5 Summary statistics of transit time (hr) for outbound migrations of Chinook salmon smolts..

	Fixed Effect: Cable Active Yes								
	Reach 1 Benicia to Richmond			Reach 2 Richmond to Golden Gate			Reach 3 Benicia to Golden Gate		
	No Cable	**Cable Active**	**Unknown**	**No Cable**	**Cable Active**	**Unknown**	**No Cable**	**Cable Active**	**Unknown**
Mean	52.47	41.28	43.57	19.50	17.03	16.32	73.83	65.69	58.07
Standard Error	2.39	3.41	2.77	1.82	2.40	2.99	2.66	5.96	3.81
Median	41.20	33.03	31.92	13.84	13.42	10.41	64.29	56.41	46.34
Standard Dev.	37.16	27.89	35.29	23.21	14.61	31.95	38.58	43.37	43.07
Sample Var.	1380.74	777.78	1245.12	538.80	213.41	1020.57	1488.69	1880.53	1855.26
Minimum	11.78	10.43	12.25	2.68	3.41	2.44	26.12	25.95	23.29
Maximum	277.20	140.93	223.36	253.66	87.34	309.54	279.50	273.58	332.54
Count	241.00	67.00	162.00	163.00	37.00	114.00	210.00	53.00	128.00

Table 4-6
Summary statistics of transit time (hr) for outbound migrations of Chinook salmon smolts.

	Reach 1 Carquinez to Richmond			Reach 2 Richmond to Golden Gate		
	No Cable	**Cable Active**	**Unknown**	**No Cable**	**Cable Active**	**Unknow**
Mean	26.11	68.51	44.61	10.72	12.79	
Standard Error	1.38	28.61	23.35	0.69	1.36	
Median	24.15	22.84	22.88	10.81	10.45	
Standard Dev.	10.02	234.16	119.04	5.00	10.94	
Sample Var.	100.44	54828.85	14170.44	25.02	119.62	
Minimum	11.24	4.75	4.49	2.78	2.44	
Maximum	49.05	1526.73	626.71	27.84	75.43	
Count	53.00	67.00	26.00	53.00	65.00	

Table 4-7
Summary statistics of transit time (hr) data for outbound migrations of adult green sturgeon.

	Reach 1 Golden Gate to Richmond			Reach 2 Richmond to Carquinez			Reach 3 Golden Gate to Carquinez		
	No Cable	**Cable Active**	**Unknown**	**No Cable**	**Cable Active**	**Unknown**	**No Cable**	**Cable Active**	**Unknown**
Mean	36.91	30.67	18.41	60.55	30.01	25.24	115.23	69.94	51.24
Standard Error	15.88	15.04	2.89	31.24	2.92	5.23	34.61	16.49	5.92
Median	14.11	13.21	16.43	31.88	21.13	24.97	58.88	51.21	51.88
Standard Dev.	63.54	103.11	8.67	121.01	20.02	13.83	142.71	110.63	15.66
Sample Var.	4037.18	10631.44	75.13	14642.71	400.79	191.26	20366.17	12238.89	245.14
Minimum	3.78	3.32	4.41	14.95	10.13	3.52	30.27	21.06	26.29
Maximum	268.51	718.96	29.24	496.21	123.02	49.61	547.33	781.40	72.37
Count	16.00	47.00	9.00	15.00	47.00	7.00	17.00	45.00	7.00

Cable activity was not a fixed effect in any best fit linear mixed model of transit times for outbound LFC smolts (Table 4-8). However, Welch t-test comparisons of transit rate indicated that cable activity may still somewhat influence smolt migrations. Tests revealed that transit rates between Benicia Bridge and Richmond Bridge (*Reach 1*) were significantly higher after the cable was active (M = 1.23, SD = 0.65) than before (M = 0.97, SD = 0.48) (t (91.15) = -2.99, p = 0.0036, Figure 4-2), implying that fish displayed a faster rate of movement in this section of the San Francisco Bay after activation. However, there was no significant difference in transit rates between Richmond Bridge and Golden Gate (*Reach 2*) before (Mdn = 0.94) versus after (Mdn =1.00) the cable was active (U = 2551, p = 0.788, Figure 4-2). When examining transit through the entire length of San Francisco Bay from Benicia Bridge to Golden Gate (*reach 3*), there was a strong but non-significant trend for transit rates to be higher when the cable was active (M = 0.98, SD = 0.39) than when not active (M = 0.87, SD = 0.38) (t (79.30) = -1.92, p = 0.058, Figure 4-2). Furthermore, although there was no significant difference in transit rates through *Reach 3* between smolts that crossed the cable location (M = 0.96, SD = 0.39) versus smolts that did not (M = 1.00, SD = 0.37), (t (39.06) = 0.56, p = 0.58), transit rates within this reach were significantly slower when smolts were detected at Bay Bridge (M = 0.84, SD = 0.37) than when they were not detected there before successfully exiting at Golden Gate (M =1.02, SD = 0.45) (t (274.89) = 4.18, p <0.0001). However, none of these tests remained significant after the removal of extreme outliers from the dataset. Although this appears to indicate that cable activity may not impact smolt transit rates, it is critical to emphasize that the removal of outliers must be biologically justified so that relevant and important data is not lost.

Table 4-8
Candidate model selection for predictors of transit time by outbound Chinook smolts through three reaches.

Candidate models using linear mixed model regression are ordered by their Akaike's Information Criterion (AIC) score. The best model (in bold) for each species and migration type was determined based on AIC comparison and log likelihood tests. Information provided includes the fixed and random effects for each candidate model as well as the number of parameters (k), the AIC score, and the log likelihood (logLik) values.

Reach	Models	k	AIC	logLik
Reach 1 (Benicia to Richmond)	t1~T+D+(1|Year)	5	2783.4	-1386.7
	t1~T+D+CC+(1|Year)	6	2784.9	-1386.5
	t1~D+(1|Year)	4	2785.1	-1388.5
	t1~T+D+C+CC+(1|Year)	7	2786.9	-1386.4
	t1~T+D+K+C+CC+(1|Year)	8	2788.8	-1386.4
	t1~T+D+RL+K+C+CC+(1|Year)	10	2792.6	-1386.3
	t1~1+(1|Year), Null	3	2796.9	-1395.5
Reach 2 (Richmond to Golden Gate)	**T2~MD+(1|Year)**	4	1610.2	-801.12
	t2~C+MD+(1|Year)	5	1610.6	-800.32
	t2~D+C+MD+(1|Year)	6	1611.3	-799.65
	t2~D+C+CC+MD+(1|Year)	7	1612.5	-799.22
	t2~T+D+C+CC+MD+(1|Year)	8	1613.9	-798.95
	t2~T+D+K+C+CC+MD+(1|Year)	9	1615.7	-798.84
	t2~1+(1|Year), Null	3	1616.4	-805.12
	t2~T+D+RL+K+C+CC+MD+(1|Year)	11	1619.6	-798.81
Reach 3 (Benicia to Golden Gate)	t3~T+D+RL+(1|Year)	7	2372.3	-1179.1
	t3~T+D+RL+MD+(1|Year)	8	2372.3	-1178.1
	t3~T+RL+(1|Year)	6	2372.9	-1180.5
	t3~T+D+RL+K+MD+(1|Year)	9	2372.9	-1177.4
	t3~T+D+RL+K+C+MD+(1|Year)	10	2374.9	-1177.4
	t3~1+(1|Year), Null	3	2376.6	-1185.3
	t3~T+D+RL+K+C+CC+MD+(1|Year)	11	2376.8	-1177.4

C = cable active (n/y), CC = cable cross (n/y), D = discharge, K = K factor, MD = misdirect (n/y), RL = release location, t1 = transit time reach 1, t2 = transit time reach 2, t3 = transit time reach 3, T = temperature.

Cable activity was a significant predictor of transit time during outbound migrations of adult green sturgeon as the best fit model of transit time through the estuary from Carquinez to Golden Gate (*Reach 3*) included both cable activity and discharge as fixed effects (Table 4-9). The average transit time through the estuary was significantly increased by 96 hours when the cable was active (ß = 96.01, p = 0.032) and discharge showed a weak but positive trend with transit time (ß = 0.06, p = 0.061). The best fit model for transit times in the first reach was the null model while the best fit model for the second reach was the full model of cable activity, release

location, misdirection, temperature, and discharge. After extreme outliers were removed, the model for the first reach retained temperature as a fixed effect (ß = -0.36, p = 0.025), the second reach model only retained misdirection as a fixed effect (ß = 7.27, p < 0.001), and the third reach model lost all fixed effects. However, as green sturgeon can display high variability in their movements within the bay, it would be presumptuous to remove these outliers.

Table 4-9
Candidate model selection for predictors of transit time by outbound adult green sturgeon through three reaches.

Candidate models using linear regression are ordered by their Akaike's Information Criterion (AIC) score. The best model (in bold) for each species and migration type was determined based on AIC comparison and log likelihood tests. Information provided includes the fixed and random effects for each model as well as the number of parameters (k), the AIC score, and the log likelihood (logLik) values.

Reach	Models	k	AIC	logLik
Reach 1 (Carquinez to Richmond)	t1~D+(1|ID)+(1|Year)	5	1458.3	-724.18
	t1~1+(1|ID)+(1|Year), Null	4	1459.2	-725.59
	t1~D+C+(1|ID)+(1|Year)	6	1459.5	-723.73
	t1~T+D+C+(1|ID)+(1|Year)	7	1461.4	-723.72
	t1~T+D+C+RL+(1|ID)+(1|Year)	9	1464.8	-723.41
Reach 2 (Richmond to Golden Gate)	**t2~T+D+C+RL+MD+(1|ID)+(1|Year)**	10	764.07	-372.04
	t2~MD+(1|ID)+(1|Year)	5	775	-382.5
	t2~T+MD+(1|ID)+(1|Year)	6	776.16	-382.08
	t2~T+C+MD+(1|ID)+(1|Year)	7	777.66	-381.83
	t2~T+D+C+MD+(1|ID)+(1|Year)	8	779.63	-381.82
	t2~1+(1|ID)+(1|Year), Null	4	785.28	-388.64
Reach 3 (Carquinez to Golden Gate)	t3~T+D+ C+(1|ID)+(1|Year)	7	1517.8	-751.88
	t3~D+C+(1|ID)+(1|Year)	6	1518.9	-753.44
	t3~T+D+C+MD+(1|ID)+(1|Year)	8	1519.3	-751.66
	t3~C+(1|ID)+(1|Year)	5	1520.3	-755.14
	t3~1+(1|ID)+(1|Year), Null	4	1521.1	-756.56
	t3~T+D+RL+C+MD+(1|ID)+(1|Year)	10	1522.7	-751.34

C = cable active (n/y), CC = cable cross (n/y), D = discharge, MD = misdirect (n/y),
RL = release location, t1 = transit time reach 1, t2 = transit time reach 2, t3 = transit time reach 3, T = temperature.

While cable activity was associated with an increase in transit time of out-migrating green sturgeon through the estuary, the opposite effect was observed for inbound migrating green sturgeon. The best fit model of inbound sturgeon transit time in *Reach 3* between Golden Gate and Carquinez included cable activity (ß = -3.77, p = 0.002), temperature (ß = 7.85, p = 0.024),

and misdirection (ß = 81.88, p = 0.012) as fixed effects (Table 4-10). While both temperature and misdirection significantly increased transit time, cable activity resulted in a decrease in transit time of 3.77 hours. Similar effects of temperature (ß = 6.69, p < 0.001) and misdirection (ß = 68.84, p = 0.065) were also seen in the best fit model of reach 1 transit time, while models for transit time in *Reach 2* failed to converge (Table 4-10). After the removal of extreme outliers, cable activity remained as a fixed effect in the best fit *Reach 3* transit time model (ß = -1.05, p < 0.001) and misdirection remained as a significant predictor of transit time in *Reach 1* (ß = 10.16, p = 0.006).

Table 4-10
Candidate model selection for predictors of transit time by inbound adult green sturgeon through three reaches.

Candidate models using linear regression are ordered by their Akaike's Information Criterion (AIC) score. The best model (in bold) for each species and migration type was determined based on AIC comparison and log likelihood tests. Information provided includes the fixed and random effects for each model as well as the number of parameters (k), the AIC score, and the log likelihood (logLik) values.

Reach	Models	k	AIC	logLik
Reach 1 (Golden Gate to Richmond)	**t1~T+MD+(1|ID)+(1|Year)**	6	721.87	-354.94
	t1~T+C+MD+(1|ID)+(1|Year)	7	725.83	-355.92
	t1~T+D+C+MD+(1|ID)+(1|Year)	8	728.34	-356.17
	t1~T+(1|ID)+(1|Year)	5	731.01	-360.5
	t1~T+D+RL+C+MD+(1|ID)+(1|Year)	10	733.81	-356.91
	t1~1+(1|ID)+(1|Year), Null	4	751.94	-371.97
Reach 2 (Richmond to Carquinez)	**---Models did not converge---**			
Reach 3 (Golden Gate to Carquinez)	**t3~T+C+MD+(1|ID)+(1|Year)**	7	745.8	-365.9
	t3~T+D+C+MD+(1|ID)+(1|Year)	8	753.42	-368.71
	t3~T+D+C+RL+MD+(1|ID)+(1|Year)	10	755.08	-367.54
	t3~1+(1|ID)+(1|Year), Null	4	768.7	-380.35

C = cable active (n/y), CC = cable cross (n/y), D = discharge, MD = misdirect (n/y), RL = release location, t1 = transit time reach 1, t2 = transit time reach 2, t3 = transit time reach 3, T = temperature.

In summary, although transit times were longer when green sturgeon were detected at Bay Bridge during their migrations, cable activity was not associated with a strong increase or decrease in the proportion of migrations that included detections at Bay Bridge. In other words,

green sturgeon do not appear to be strongly 'mis-directed' by the cable from their migration route in a southward direction towards Bay Bridge, but when they are detected at Bay Bridge, they take longer to transit through the San Francisco Bay.

First Presence at Array

The best model for predicting the location of where Chinook smolts were first detected at an array during the periods of cable inactivity included the following predictor variables: distance to eventual cable location (ß = -1.31, $p < 0.0001$), channel depth (ß = 0.12, $p = 0.0006$), and total magnetic fields measured at the surface of the water (ß = 0.0007, $p = 0.004$). However, after the cable was activated, the only predictors left in the best fit model include distance to cable location (ß = -1.92, $p < 0.0001$) and channel depth (ß = 0.04, $p = 0.32$), with only distance to cable being a significant factor. In summary, before the cable was activated, Chinook were more likely to first be detected at receivers that were closer to the eventual location of the cable, higher in channel depth, and higher in total magnetic field intensity. However, after the cable was activated, only the distance to cable location was significant with fish more likely to be detected closer to the cable. These results indicate that Chinook smolts may be attracted to the activated cable.

Discussion

After the cable was activated, there was an average increase of approximately 20% in both the proportion of Chinook smolts that crossed the cable location and the proportion of smolts detected at Bay Bridge south of their normal migration route. When comparing all years of data during cable inactivity (2007-2009) vs. activity (2011), cable activation was associated with an average decrease of 11.1 % in the proportion of Chinook smolts that were able to successfully exit San Francisco Bay. However, if the unusually high survival year of 2007 is not included, there is only an average decrease in the proportion of successful exits of 2.7% after the cable is activated. Cable activity did not predict an increase in the probability of crossing the cable location or in successfully exiting the system, but it did predict an increase in the probability that LFC smolts would be misdirected to Bay Bridge. Cable activity was also not significantly related to transit time in any of the three reaches of this system. Furthermore, relationships between cable activity and transit rate in LFC were not robust. Lastly, after the cable was

activated, distance to cable remained the only significant factor predicting the first detection location of Chinook smolts at an array. Taken together, these results indicate that Chinook salmon smolts may be attracted to the cable after activation (increased probability of misdirections to the Bay Bridge, importance of closeness to cable in first presence analysis), but they do not appear to be impeded from successfully migrating through the San Francisco Bay. However, it is important to emphasize that only one year of LFC smolt data was available after the cable was activated (2011). Additional study years would be required to more confidently address the question of how high voltage direct current cables impact salmonid migrations.

In outbound migrating adult green sturgeon, cable activation was associated with a 14.9 % increase in the proportions of migrations that crossed the cable location, a 2.3 % increase in the proportion of migrations that involved detections at Bay Bridge, and a 4.0 % decrease in the proportion of successful migrations (i.e., detections at Golden Gate). Transit times of outbound migrations from Carquinez to Golden Gate were not affected by crossing the cable location but were trending towards being longer if the fish was detected at Bay Bridge and were significantly longer after cable activation versus before activation. For inbound migrating adult green sturgeon, periods of cable activity were associated with a 6.5 % decrease in the proportion of migrations that involved detections at Bay Bridge and a 1.5 % increase in the proportion of successful inbound migrations (i.e., detections at Carquinez). The proportion of migrations that involved crossing the location of the cable was not impacted by cable activation as all inbound migrations involved crossing the cable location. Transit times for the reach between Golden Gate and Carquinez were significantly longer if fish were detected at Bay Bridge and were significantly shorter during periods of cable activity versus inactivity. Overall, cable activity had opposite effects on outbound and inbound green sturgeon migrations. While outbound migrations took significantly longer after cable activation, along with a small increase in cable crossing, a very small increase misdirected movements to Bay Bridge, and a very small decrease in successful migrations to Golden Gate, inbound migrations took significantly less time after cable activation, along with a very small decrease in the number of misdirections to Bay Bridge and a very small increase in successful migrations to Carquinez. Despite the significant effect on transit time, cable activity did not strong impact the ability of green sturgeon to complete their

outbound or inbound migrations. Despite the significant effect on transit time, cable activity did not strong impact the ability of green sturgeon to complete their outbound or inbound migrations.

A question of interest is to assess the lateral distance from a vertical projection of the cable at which the contribution of the cable to the total magnetic field (cable plus earth fields) would be close to (1) the detection limits of the Geometrics G-882 Transverse Gradiometer used in the study (< 3 nT), and (2) the low range at which some marine species may possibly detect a field discrepant from background, a value on the order of 10 nT, [39]within the same order of magnitude as the floor of the magnetometer's detection range. A theoretical approach was adopted for this exercise, because the natural environment is noisy for determining exact distances for such small fields, and the basic equations that predict magnetic field anomalies from a DC power cable provide a valid way to quantify anomaly decay with distance [21]. Assuming a realistic 2 m depth of cable loaded to 1,000 A (the cables rated current) and measurement altitudes above the bay bottom of 5 m and 10 m (i.e., total vertical distances of 7 m and 12 m from cable to detector), calculations were conducted for all combinations of twist angle of the cable, and angle of the survey line (i.e., the magnetic field profile) relative to east-west in 15º increments, resulting in 576 unique angle combinations. At 5 m and 10 m measurement heights above bottom, the anomalies – the maximum excursion of the field had respective means of 543±34 (std dev) nT and 185±12 nT. Though not strictly normal, the anomaly distributions were unimodal with the means and medians virtually identical. At ±35 m from the centerline the absolute deviation of the magnetic fields were not unimodally distributed, deviating from background with a central tendency of about 10 nT, and displaying a wide dispersion. At 5 m measurement height, the median field was 11.7 nT (2.5th – 97.5th percentile range of 0.49 – 17.7 nT). At 10 m, the corresponding values were a median of 10.9 nT (2.5th – 97.5th percentile range of 0.47 – 16.5 nT). The values at the two measurement heights are similar because the net field is determined mostly by the linear projection of magnetometer to cable, which is 35.7 m for a 5-m measurement height, and 37.0 m for a 10-m measurement height. Also, because of symmetry factors, the distributions are identical at equal bilateral distances.

In order to more fully examine how intensities of this magnitude and dimensional spread may impact the normal migration or foraging behaviors of electromagnetically-receptive marine

species, it is imperative to conduct studies which investigate the sensitivity levels of these species to such fields. Laboratory tests that determine thresholds of detection and behavioral alteration would be extremely helpful as the "active space" of the cable anomaly could be modelled for different key species. In addition to lab experiments, it is also very important to conduct field studies which strive to investigate the impact of cable anomalies on the natural behavior of animals, both on small and large scales.

Here, we used a naturally occurring experiment to examine how cable activation impacted fish migration behavior across the whole of San Francisco Bay. Previous studies have investigated the response of electromagnetically-sensitive silver eels to a high voltage, direct current cable similar to the Trans Bay Cable. Westerberg and Begout-Anras (2000) found that approximately 60% of the eels monitored passed over the cable during their migration route, indicating that the cable's electromagnetic field did not act as a strong barrier to their regular migration movements. [23] An additional study examined swim speeds of silver eels in relation to an alternating current cable [24]. Here, eels slowed down significantly as they passed over the region of the cable as compared to swim speeds further away on either side of the cable. Westerberg and Lagenfeldt argued that an intensive tracking study is necessary to identify effects on a migratory species. We recommend that future tracking studies employ transmitters carrying a strain gauge and 3-axis accelerometer to characterize the swimming behavior of the fish as they pass over the cable and a 3-axis gradiometer to measure the strength of the EMF induced by current flowing through the cable. Two migratory species, the green sturgeon and cow shark (*Notorhynchus cepedianus*), have been tracked in the vicinity of the Trans Bay Cable and would make ideal candidates for such a study [25, 26].

5
REFERENCES

1. Gill, A.B., *Offshore renewable energy: ecological implications of generating electricity in the coastal zone.* Journal of Applied Ecology, 2005. **42**: p. 605-615.

2. Teo, S.L.H., et al., *Archival and acoustic tags reveal the post-spawning migrations, diving behavior, and thermal habitat of hatchery-origin Sacramento River steelhead kelts (Oncorhynchus mykiss).* Environmental Biology of Fishes, 2012. **96**: p. 175-187.

3. Heublein, J., et al., *Migration of green sturgeon, Acipenser medirostris, in the Sacramento River.* Environmental Biology of Fishes, 2009. **84**: p. 245-258.

4. Chapman, E.D., et al., *Diel movements of out-migrating Chinook salmon (Oncorhynchus tshawytscha) and steelhead trout (Oncorhynchus mykiss) smolts in the Sacramento/San Joaquin watershed.* Environmental Biology of Fishes, 2013. **96**: p. 273-286.

5. Hearn, A.R., et al., *Movements of out-migrating late-fall run Chinook salmon (Oncorhynchus tshawytscha) smolts through the San Francisco Bay Estuary.* Environmental Biology of Fishes, 2014. **97**: p. 851-863.

6. Michel, C.J., et al., *The effects of environmental factors on the migratory movement patterns of Sacramento River yearling late-fall run Chinook salmon (Oncorhynchus tshawytscha).* Environmental Biology of Fishes, 2013. **96**: p. 257-271.

7. Singer, G.P., et al., *Interannual variation of reach specific migratory success for Sacramento River hatchery yearling late-fall run Chinook salmon (Oncorhynchus tshawytscha) and steelhead trout (Onchorhynchus mykiss).* Environmental Biology of Fishes, 2013. **96**: p. 363-379.

8. Haugh, C.V. and M.M. Walker, *Magnetic discrimination learning in rainbow trout (Oncorhynchus mykiss).* Journal of Navigation, 1998. **51**: p. 35-45.

9. Quinn, T.P. and E.L. Brannon, *The use of celestial and magnetic cues by orienting sockeye salmon smolts.* Journal of Comparative Physiology, 1982. **147**: p. 547-552.

10. Quinn, T.P. and C. Groot, *Orientation of chum salmon (Oncorhynchus keta) after internal and external magnetic-field alteration.* Canadian Journal of Fisheries and Aquatic Sciences, 1983. **40**: p. 1598-1606.

11. Taylor, P.B., *Experimental-evidence for geomagnetic orientation in juvenile salmon, Oncorhynchus tschawytscha Walbaum.* Journal of Fish Biology, 1986. **28**: p. 607-623.

12. Basov, B.M., *Behavior of Sterlet Acipenser ruthenus and Russian Sturgeon A. gueldenstaedtii in Low-Frequency Electric Fields.* Journal of Ichthyology, 1999. **39**: p. 782-787.

13. Cada, G.F., et al., *Laboratory studies of the effects of static and variable magnetic fields on freshwater fish*, 2012, Oak Ridge National Laboratory: Oak Ridge, Tennessee. p. 42.

14. Teeter, J.H., R.B. Szamier, and M.V.L. Bennett, *Ampullary electroreceptors in the sturgeon Scaphirhynchus platorynchus (Rafinesque).* Journal of Comparative Physiology, 1980. **138**: p. 213-223.

15. Klimley, A.P., *Highly directional swimming by scalloped hammerhead sharks, Sphyrna lewini, and subsurface irradiance, temperature, bathymetry, and geomagnetic field.* Mar Biol, 1993. **117**: p. 1-22.

16. Gove, P., *Webster's Third New International Dictionary of the English Language*1966, Springfield, Massachusetts: G & C Merriam Co.

17. Klinowska, M., *Cetacean live stranding sites relate to geomagnetic topography.* Aquatic Mammals, 1985. **1**: p. 27-32.

18. Kirschvink, J.L., A.E. Dizon, and J.A. Westphal, *Evidence from stranding for geomagnetic sensitivity in cetaceans.* Journal of Exposure Biology, 1986. **120**: p. 1-24.

19. Thomas, M.J., et al., *Behavior, movements, habitat use of adult green sturgeon, Apicenser medirostris, in the upper Sacramento River.* Environmental Biology of Fishes, 2014. **97**: p. 133-146.

20. Tricas, T.C. and B.A. Carlson, *Electroreceptors and magnetoreceptors*, in *Cell Physiology Sourcebook*, Elsevier. p. 705-725.

21. Kavet, R., M.T. Wyman, and A.P. Klimley, *Modeling Magnetic Fields from a DC Power Cable Buried Beneath San Francisco Bay Based on Empirical Measurements.* PloS one, 2016. **11**(2): p. e0148543.

22. Tchernychev, M., *MAGPICK - magnetic map and profile processing. User Guide. Online access: ftp://geom.geometrics.com/pub/mag/Manuals/MagPick.pdf* 2013.

23. Westerberg, H. and M.L. Begout-Anras, *Orientation of silver eel (Anguilla Anguilla) in a disturbed geomagnetic field*, in *Advances in Fish Telemetry*, R. Moore A, Editor 2000, CFAS: Norwich, England. p. 149-375.

24. Westerberg, H. and I. Lagenfelt, *Sub-sea power cables and the migration behaviour of the European eel.* Fish Mgmt Ecol, 2008. **15**: p. 369-375.

25. Kelly, J.T., A.P. Klimley, and C.E. Crocker, *Movements of green sturgeon, Acipenser mediostris, in the San Francisco Estuary, California.* Environ Biology Fish, 2007. **79**: p. 281-295.

26. Buckhorn, M.L., et al., *Tidally assisted movements of sevengill sharks in San Francisco Bay.* Anim Biotel, 2016. **Submitted**.

27. EPRI, *EPRI Workshop on EMF and Aquatic Life.*, 2013, EPRI: Palo Alto, California. Product ID: 3002000477.

28. Boehlert, G.W. and A.B. Gill, *Environmental and Ecological Effects Of Ocean Renewable Energy Development: A Current Synthesis.* Oceanography, 2010. **23**: p. 68-81.

29. Klimley, A.P., M.T. Wyman, and R. Kavet, *Chinook salmon and green sturgeon migrate through San Francisco Estuary despite large distortions in the local magnetic field produced by bridges.* PloS one, 2016. In revision**.**

30. Fulton, T., *Rate of growth of sea fishes.* Sci Invest Fish Div Scotl Rep, 1902. **20**.

31. Bivand, R. and N. Lewin-Koh, *maptools: Tools for Reading and Handling Spatial Objects: Available at: https://CRAN.R-project.org/package=maptools*, in *R package version 0.8-39*.

32. Van Eenennaam, J.P., et al., *Reproductive Conditions of the Klamath River Green Sturgeon.* Transactions of the American Fisheries Society, 2006. **135**: p. 151-163.

33. Erickson, D.L. and M.A.H. Webb, *Spawning periodicity, spawning migration, and size at maturity of green sturgeon, Acipenser medirostris, in the Rouge River, Oregon.* Environ Biol Fish, 2007. **79**: p. 255-268.

34. Perry, R.W., et al., *Using mark-recapture models to estimate survival telemetry data*, in *Telemetry Techniques: A User Guide for Fisheries Research*2012, American Fisheries Society.

35. Mazerolle, M.J., *AICcmodavg: Model selection and multimodel inference based on (Q)AIC(c) : Available at: https://CRAN.R-project.org/package=lmerTest*, in *R package version 2.0-4*2016.

36. R Core Team, *R: A language and environment for statistical computing: Available at: https://www.R-project.org/*, R Foundation for Statistical Computing, Editor 2016.

37. Wickham, H., *ggplot2: Elegant Graphics for Data Analysis*2009, New York, New York: Springer-Verlag.

38. Bates, D., et al., *Fitting Linear Mixed-Effects Models Using lme4.* Journal of Statistical Software, 2015. **67**(1): p. 1-48.

39. Normandeau, E., T.C. Tricas, and A.B. Gill, *Effects of EMFs from Undersea Power Cables on Elasmobranchs and Other Marine Species.*, 2011, U.S. Dept. of the Interior, Bureau of Ocean Energy Management, Regulation, and Enforcement, Pacific OCS Region. OCS Study BOEMRE 2011-09. Available at: http://www.hawaii.edu/fishlab/pubs/Normandeau%20Associates%20et%20al.%202011.pdf: Camarillo, CA. .

6 ACKNOWLEDGMENTS

This study was funded by the US Department of Energy, Office of Energy Efficiency and Renewable Energy, award no. DE-EE0006382 and by the US Department of the Interior, Bureau of Ocean Energy Management, Environmental Studies Program, Washington, DC, through Interagency Agreement Number M14PG00012. EPRI support was funded through a cost share agreement with the Electric Power Research Institute (Project 1–105902).

We would like to kindly thank Trans Bay Cable LLC for providing cable load data for our study. We also thank the boat operators and crew who helped conduct the gradiometer survey and the staff at Geometrics for their training and support. The scope of this project would not be possible without the kind permission to use fish detection data from National Oceanic and Atmospheric Administration, National Marine Fisheries Service, US Bureau of Reclamation, California Department of Water Resources, California Department of Fish and Wildlife, Oregon Department of Fish and Wildlife, Washington Department of Fish and Wildlife, US Fish and Wildlife, East Bay Municipal Utility District, US Army Corps of Engineers, and H.T. Harvey and Associates.